Geochemistry, Geophysics, Geosystems®

AGU ADVANCING EARTH AND SPACE SCIENCE

RESEARCH ARTICLE
10.1029/2022GC010519

Earth's Earliest Phaneritic Ultramafic Rocks: Mantle Slices or Crustal Cumulates?

Jiawei Zuo[1], A. Alexander G. Webb[1], Emily J. Chin[2], Lukáš Ackerman[3], Jason Harvey[4], Peter J. Haproff[5], Thomas Müller[6], Qin Wang[7], Arthur H. Hickman[8], Dominik Sorger[6], and Anthony Ramírez-Salazar[4]

[1]Department of Earth Sciences and Laboratory for Space Research, University of Hong Kong, Hong Kong, China, [2]Scripps Institution of Oceanography, University of California, San Diego, La Jolla, CA, USA, [3]Institute of Geology of the Czech Academy of Sciences, Prague 6, Czech Republic, [4]School of Earth and Environment, University of Leeds, Leeds, UK, [5]Department of Earth and Ocean Sciences, University of North Carolina Wilmington, Wilmington, NC, USA, [6]Department of Mineralogy, Geoscience Center, Georg-August-Universität Göttingen, Göttingen, Germany, [7]State Key Laboratory for Mineral Deposits Research, School of Earth Sciences and Engineering, Nanjing University, Nanjing, China, [8]Geological Survey of Western Australia, East Perth, WA, Australia

Key Points:

- Isua and Pilbara ultramafic rocks interacted with low Pt and Pd lavas from deep, potentially reduced mantle and/or magma chambers
- Isua and Pilbara ultramafic rocks are geochemically similar and can be interpreted as crustal cumulates
- Isua and Pilbara ultramafic rocks can form in either plate or non-plate tectonic settings, thus do not require >3.2 Ga subduction

Supporting Information:

Supporting Information may be found in the online version of this article.

Correspondence to:

J. Zuo and A. A. G. Webb,
jwzuo@connect.hku.hk;
aagwebb@hku.hk

Citation:

Zuo, J., Webb, A. A. G., Chin, E. J., Ackerman, L., Harvey, J., Haproff, P. J., et al. (2022). Earth's earliest phaneritic ultramafic rocks: Mantle slices or crustal cumulates? *Geochemistry, Geophysics, Geosystems*, *23*, e2022GC010519. https://doi.org/10.1029/2022GC010519

Received 24 MAY 2022
Accepted 11 NOV 2022

Abstract When plate tectonics initiated remains uncertain, partly because many signals interpreted as diagnostic of plate tectonics can be alternatively explained via hot stagnant-lid tectonics. One such signal involves the petrogenesis of early Archean phaneritic ultramafic rocks. In the Eoarchean Isua supracrustal belt (Greenland), some phaneritic ultramafic rocks have been dominantly interpreted as subduction-related, tectonically-exhumed mantle slices or cumulates. Here, we compared Eoarchean phaneritic ultramafic rocks from the Isua supracrustal belt with mantle peridotites, cumulates, and phaneritic ultramafic samples from the Paleoarchean East Pilbara Terrane (Australia), which is widely interpreted to have formed in non-plate tectonic settings. Our findings show that Pilbara samples have cumulate and polygonal textures, melt-enriched trace element patterns, relative enrichment of Os, Ir, and Ru versus Pt and Pd, and chromite-spinel with variable TiO_2 and Mg#, and relatively consistent Cr#. Both, new and existing data show that cumulates and mantle rocks potentially have similar whole-rock geochemical characteristics, deformation fabrics, and alteration features. Geochemical modeling results indicate that Isua and Pilbara ultramafic rocks have interacted with low-Pt and Pd melts generated by sequestration of Pd and Pt into sulphide and/or alloy during magmatism. Such melts cannot have interacted with a mantle wedge. Correspondingly, geochemical compositions and rock textures suggest that Isua and Pilbara ultramafic rocks are not tectonically-exhumed mantle peridotites, but are cumulates that experienced metasomatism by fluids and co-genetic melts. Because such rocks could have formed in either plate or non-plate tectonic settings, they cannot be used to differentiate early Earth tectonic settings.

Plain Language Summary Earth's rigid outer shell is broken into rigid pieces that move relative to each other. These motions are generally understood to reflect plate tectonics. However, the origins of plate tectonics are poorly understood. This contribution focuses on an aspect of this problem: the lack of consensus concerning when plate tectonics started. We examine some of the oldest rocks on Earth that researchers have speculated record plate tectonic processes: ultramafic rocks from the ≥3.7 billion-years-old Isua supracrustal belt of southwestern Greenland. A leading hypothesis suggests that these rocks are slices of mantle emplaced by plate tectonic deformation. We test the viability of an alternative hypothesis that they may have crystallized from magmas at shallow crustal levels, which does not require a plate tectonics setting. Specifically, we compare new and published mineral and chemical features of the Isua ultramafic rocks with similar rocks from known crustal and mantle settings, including new data from similarly ancient terrane in northwestern Australia that is widely considered to be non-plate tectonic. Results show that each feature of the Isua ultramafic rocks is consistent with crustal crystallization. Therefore, these ultramafic rocks do not constrain early plate tectonics, which could have developed later.

1. Introduction

When, how, and why plate tectonics began on Earth remain among the most important unresolved questions in plate tectonic theory (e.g., Bauer et al., 2020; Beall et al., 2018; Harrison, 2009; Korenaga, 2011; Nutman

et al., 2020; Stern, 2008; Tang et al., 2020). Investigations of plate tectonic initiation have significant implications for questions associated with the evolution of early terrestrial planets, including whether early Earth experienced any pre-plate tectonic global geodynamics/cooling after the magma ocean stage (e.g., Bédard, 2018; Collins et al., 1998; Lenardic, 2018; Moore & Webb, 2013; O'Neill & Debaille, 2014), and why other terrestrial planets in the solar system appear to lack plate tectonic records (e.g., Moore et al., 2017; Stern et al., 2017; cf. Yin, 2012a, 2012b).

Many proposed signals for the initiation or early operation of plate tectonics on Earth are controversial due to the issue of their non-uniqueness. For instance, the origin of Hadean zircons from the Jack Hills of western Australia has been contrastingly interpreted as detritus from Hadean felsic arc magmas (Harrison, 2009; Hopkins et al., 2008), bolide impact processes (Marchi et al., 2014), or low-pressure crust partial melts (Reimink et al., 2020). Similarly, it is debated whether the Archean high Al_2O_3/TiO_2 mafic lavas (also known as boninites or boninitic basalts) indicate the initiation of Eoarchean subduction (cf. Pearce & Reagan, 2019; Polat & Hofmann, 2003). Another example is how a ∼3.2 Ga shift in zircon Hf-isotope signatures has been variably interpreted to indicate the onset of plate tectonics (Næraa et al., 2012) or a proposed mantle thermal peak (Kirkland et al., 2021). There are geological records that remain widely considered unique to plate tectonics (e.g., paired metamorphic belts, ultra-high pressure [UHP] terranes, and passive margins); these are consistent with a ≤3.2 Ga initiation of plate tectonics (e.g., Brown & Johnson, 2018; Cawood et al., 2018; Stern, 2008; cf. Bauer et al., 2020; Foley et al., 2014; Harrison, 2009; Korenaga, 2011; Nutman et al., 2020). This interpretation requires some form of single-plate stagnant-lid tectonics to predate plate tectonics (e.g., Bédard, 2018; Collins et al., 1998; Moore & Webb, 2013).

One proposed signal of early plate tectonics is the preservation of phaneritic ultramafic rocks in Eo- and Paleoarchean terranes. In the Eoarchean Isua supracrustal belt and adjacent meta-tonalite bodies exposed in southwestern Greenland (Figure 1a), some meta-dunites and meta-harzburgites have been interpreted to represent thrust-emplaced mantle rocks that experienced mantle wedge deformation, UHP metamorphism, and/or metasomatization involving arc basaltic melts (e.g., Friend & Nutman, 2011; Kaczmarek et al., 2016; Nutman et al., 2020; Van de Löcht et al., 2018), similar to how modern ophiolitic ultramafic rocks form in the mantle and are preserved in collisional massifs (e.g., Boudier et al., 1988; Lundeen, 1978; Wal & Vissers, 1993). However, these processes are not compatible with proposed non-plate tectonic origins for the Isua supracrustal belt, where both mantle wedge and tectonic exhumation of the mantle are not predicted, such that the ultramafic rocks can only be cumulates or high-Mg extrusive rocks (e.g., komatiites) without UHP metamorphic overprints and melt-rock interactions involving arc magmas (Ramírez-Salazar et al., 2021, 2022; Webb et al., 2020). Although Szilas et al. (2015) and Waterton et al. (2022) argue that dunites and harzburgites in the Isua supracrustal belt can be interpreted as crustal cumulates formed by fractionation of Isua basalts, additional examinations are required to rule out the necessity of plate tectonics to explain their petrogenesis and metamorphic history. Namely, further investigations of the igneous and metamorphic features of Isua ultramafic rocks, origins of their potential parent melts, and natures of melt/fluid components that have interacted with the rocks (Friend & Nutman, 2011; Van de Löcht et al., 2020; Waterton et al., 2022) are necessary outstanding tests. If Isua ultramafic rocks are cumulates or high-Mg lavas that have not experienced alteration and deformation unique to plate tectonic settings, then the rocks cannot be used as unequivocal indicators of plate tectonics and tests of early Earth tectonic models.

In this contribution, we explore the origins of Isua ultramafic rocks through comparative analysis of new and existing geochemical and petrological data, including analysis of key Isua samples and rocks of a similar lithology from settings considered representative of hot stagnant-lid tectonics (In this study, we follow tectonic taxonomy from Lenardic (2018)). The Paleoarchean geology of the East Pilbara Terrane of western Australia is widely accepted as representing hot stagnant-lid tectonics (Hickman, 2021; Johnson et al., 2014; Smithies et al., 2007, 2021; Van Kranendonk et al., 2004, 2007), and Pilbara ultramafic samples are used in this study (Figure 1b) as examples of ultramafic rocks from non-plate tectonic regimes. The petrographic and geochemical features of Pilbara ultramafic samples and (modeled) cumulates are compared with those of tectonically exhumed mantle peridotites to explore similarities and discriminating differences between mantle slices and phaneritic ultramafic rocks that are compatible with non-plate tectonic settings. We compare Pilbara ultramafic samples with Isua ultramafic samples to explore whether their differences require contrasting protolith origins or reflect different alteration overprints. We then address whether the Isua and Pilbara ultramafic rocks could be viably interpreted to be crustal cumulates, or must be interpreted as tectonically exhumed mantle peridotites. Finally, we

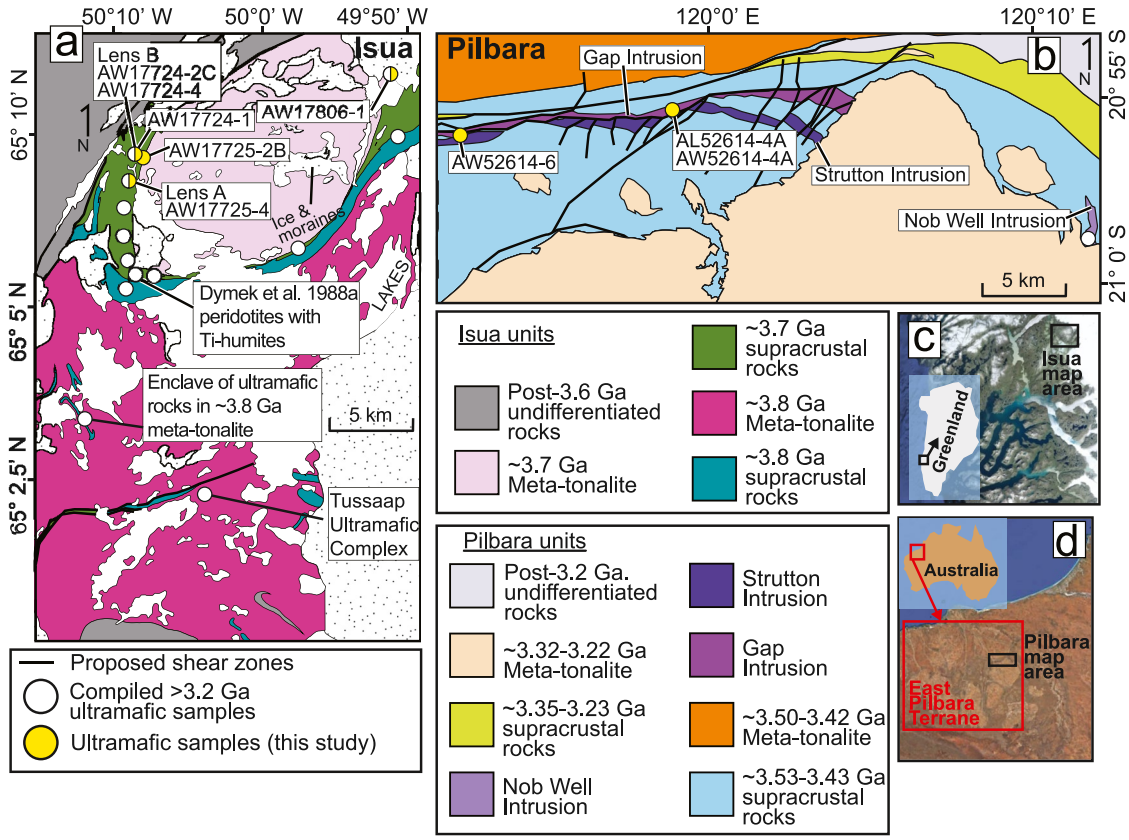

Figure 1. Geological maps of the Isua supracrustal belt, southwestern Greenland and the east-central portion of the East Pilbara Terrane, northwestern Australia. (a) simplified geology of the Isua supracrustal belt and adjacent areas (modified from Nutman et al. (2002)). Locations of meta-peridotite enclaves and lenses A and B are presented. (b) simplified geology of the north edge of the Mount Edgar Complex (modified from Van Kranendonk et al., 2007) showing major km-scale Paleoarchean ultramafic intrusive bodies: the Gap Intrusion, Nob Webb Intrusion, and Strutton Intrusion. See Figure S1 in Supporting Information S1 for the geology of the whole East Pilbara Terrane. (c) Location of the Isua supracrustal belt in southwestern Greenland. (d) Location of the East Pilbara Terrane in northwestern Australia. Yellow circles: locations for new samples; white circles, locations for compiled samples from Szilas et al. (2015), Van de Löcht et al. (2018), Friend et al. (2002), Friend and Nutman (2011), McIntyre et al. (2019), Dymek, Boak, and Brothers (1988), and the Geological Survey of Western Australia 2013 database (2013).

explore the geodynamic implications of the petrogenesis of Isua and Pilbara ultramafic rocks, thereby assessing whether plate tectonics is required to explain the early Archean evolution of Earth and initiated prior to ~3.8 Ga.

2. Geological Background and Proposed Tectonic Models

2.1. The Isua Supracrustal Belt, Southwestern Greenland

The ~35-km-long and ~1–4-km-wide Isua supracrustal belt of southwestern Greenland is Earth's largest recognized Eoarchean terrane (Figure 1a). The protoliths of the belt formed dominantly at ~3.8 and ~3.7 Ga, and subsequently experienced extensive shearing, thinning, and folding (e.g., Nutman et al., 2020; Webb et al., 2020). Regional deformation of the Isua supracrustal belt is associated with amphibolite-facies assemblages that have been interpreted to be Eoarchean (e.g., Nutman et al., 2020; Ramirez-Salazar et al., 2021; Webb et al., 2020; Zuo, Webb, Piazolo, et al., 2021) and/or Neoarchean in age (e.g., Chadwick, 1990; Nutman, 1986; Nutman et al., 2015). Meta-tonalites of ~3.8 and ~3.7 Ga ages are in contact with the Eoarchean supracrustal belt to the north and south (Crowley, 2003; Crowley et al., 2002). The interior of the belt exposes metamorphosed basalts (a high Al_2O_3/TiO_2 "boninitic" series and a low Al_2O_3/TiO_2 "tholeiitic" series; Szilas et al., 2015), chert, banded iron formation, and minor metamorphosed ultramafic igneous rocks, felsic volcanic rocks, and detrital sedimentary rocks (e.g., Nutman & Friend, 2009; Nutman et al., 2002).

Ultramafic rocks in the Isua supracrustal belt appear to have experienced various degrees of alteration including carbonitization and serpentinization (e.g., Dymek, Brothers, & Schiffries, 1988; Friend et al., 2002; Szilas

et al., 2015). Ultramafic rocks within two ~10^4 m^2 meta-peridotite lenses (lens A in the south and lens B in the north), located ~1.5-km apart along the eastern edge of the western Isua supracrustal belt, and some ultramafic enclaves (as large as ~10^4 m^2) within meta-tonalites, located ~15 km south of the belt (Figure 1a), preserve phaneritic olivine crystals, and thus are generally considered to be least altered (e.g., Friend et al., 2002; Friend & Nutman, 2011; Nutman & Friend, 2009; Szilas et al., 2015). Previous research shows that these ultramafic rocks have (a) primary polygonal textures overprinted by B-type olivine deformation fabrics (dunites from lenses A and B; Kaczmarek et al., 2016; Nutman et al., 1996); (b) a mineral assemblage of olivine + serpentine ± pyroxene ± Ti-humite ± carbonate ± spinel ± ilmenite ± magnesite for dunites from lenses A and B (e.g., Guotana et al., 2022; Nutman et al., 2020; Szilas et al., 2015) and a mineral assemblage of olivine + serpentine + pyroxene + spinel ± hornblende for meta-peridotites from the ultramafic enclaves (Van de Löcht et al., 2018, 2020); (c) primitive mantle-normalized rare earth element patterns (REE) that are sub-parallel to those of nearby basalts (e.g., Szilas et al., 2015; Van de Löcht et al., 2020) or komatiite (Dymek, Brothers, & Schiffries, 1988); and (d) various highly siderophile element (HSE) patterns, including relatively high primitive mantle-normalized Os, Ir, and Ru versus Pt and Pd preserved in ultramafic enclaves within the southern meta-tonalite (Van de Löcht et al., 2018), and similar patterns preserved in lenses A and B (Waterton et al., 2022).

The presence of meta-peridotites in the Isua supracrustal belt and adjacent tonalite enclaves has been used to support a plate tectonic origin for the belt (e.g., Friend & Nutman, 2011; Nutman et al., 2020; Van de Löcht et al., 2020), with these dunites being interpreted as mantle rocks emplaced into the crust in an Eoarchean subduction setting (see Figure 8 of Nutman et al., 2013). In this context, Isua phaneritic ultramafic rocks were originally olivine ± pyroxene ± spinel mantle residues, which then experienced deformation, serpentinization, UHP metamorphism, as well as melt-metasomatism in an Eoarchean mantle wedge, such that they preserve B-type olivine fabrics, Ti-humite, variably fractionated HSE patterns, REE patterns parallel to those of nearby basalts, and/or olivine with clinopyroxene inclusions and mantle-like oxygen isotopes (e.g., Friend & Nutman, 2011; Nutman et al., 2020; Nutman, Scicchitano, et al., 2021). After crustal emplacement, these rocks experienced additional metamorphism, carbonitization and serpentinization during regional tectonothermal events (e.g., Guotana et al., 2022; Nutman, Scicchitano, et al., 2021).

In an alternative to plate tectonics, Webb et al. (2020) proposed a form of hot stagnant-lid tectonics, termed the heat-pipe model, for the formation and deformation of the Isua supracrustal belt. Evidence suggests that heat-pipe tectonics is currently dominant for Jupiter's moon Io and may have occurred on all hot terrestrial planets, including the early Earth (e.g., Moore & Webb, 2013; Moore et al., 2017; O'Reilly & Davies, 1981; Zuo, Webb, Johnson, et al., 2021). Heat-pipe tectonics involves rapid heat and material transport driven by voluminous global volcanism. Downwards volcanic advection (i.e., burial) of cold surface rocks permitted deformation, chilling of geothermal gradient, efficient crustal reworking, tonalite petrogenesis, and material exchanges between the surface and mantle (Bland & McKinnon, 2016; Moore & Webb, 2013; cf. Nutman, Bennett, et al., 2021). The termination of heat-pipe tectonics could be associated with plate-breaking and plate tectonic initiation events, leading to further deformation and metamorphism (Moore & Webb, 2013; Tang et al., 2020). With respect to the formation of ultramafic rocks, due to the lack of subduction processes, the heat-pipe model does not involve metasomatism by co-genetic arc-derived melts and subsequent thrust emplacement of mantle peridotites. Instead, all Isua ultramafic rocks would represent altered, high-Mg lavas or crustal cumulates. In this context, the geochemical signatures of Isua phaneritic ultramafic rocks were controlled by parental melt compositions, fractional crystallization, and alterations by fluids/melts of non-subduction origins. Ultramafic rock textures were produced by crystallization of melts and/or subsequent deformation/mineral re-equilibration under crustal conditions. Metamorphic mineral assemblages observed in Isua ultramafic rocks were formed under amphibolite-facies conditions, consistent with other parts of the belt (e.g., Ramírez-Salazar et al., 2021, 2022; cf. Friend & Nutman, 2011; Nutman et al., 2020).

2.2. The East Pilbara Terrane

The ~40,000 km^2 East Pilbara Terrane of northwestern Australia is Earth's largest and best-preserved Paleoarchean terrane (Figure 1b and Figure S1 in Supporting Information S1). There, 11 granitoid bodies consisting of mostly meta-tonalites and minor granites are surrounded by broadly coeval supracrustal belts. These supracrustal belts are dominantly comprised of metamorphosed bimodal volcanic rocks, with some chemical and clastic sedimentary rocks and layered ultramafic volcanics and intrusions (e.g., Hickman, 2021; Van Kranendonk et al., 2007). Previous studies show that by the end of the Paleoarchean, East Pilbara supracrustal belts had

been deformed into synformal keels and granitoids had been warped into domes (e.g., Collins et al., 1998; Hickman, 2021; Van Kranendonk et al., 2007). This regional "dome-and-keel" geometry is a key element for tectonic interpretations of the East Pilbara Terrane.

Ultramafic rocks of the East Pilbara Terrane occur as layers and pods interleaved with supracrustal rocks and kilometer-scale igneous bodies intruding supracrustal sequences (e.g., Smithies et al., 2007). Ultramafic layers and pods found in the supracrustal sequences commonly have thicknesses of ∼1–5 m and in some cases preserve spinifex textures. These ultramafic rocks have been interpreted to have been crystallized from komatiitic or basaltic lava flows (e.g., Smithies et al., 2007; Van Kranendonk et al., 2007). In this study, we focus on three >10-km-long and >100-m-thick ultramafic intrusive bodies that are older than ∼3.2 Ga, which include the Gap Intrusion, Strutton Intrusion, and Nob Well Intrusion (Figure 1b). These ultramafic bodies intrude ∼3.53–3.43 Ga supracrustal sequences and are intruded themselves by ∼3.31 Ga granodiorites (Figure 1b) (Williams, 1999). Existing knowledge of these ultramafic rocks is mostly limited to map relationships, petrological descriptions, and geochemical data published by the Geological Survey of Western Australia (e.g., Williams, 1999). In general, these ultramafic intrusions are comprised of variably altered peridotite (including dunite), pyroxenite, and gabbro (Geological Survey of Western Australia, 2013 Database, 2013).

Most researchers interpret that East Pilbara Terrane represents a Paleoarchean terrane formed via regional hot stagnant-lid tectonics featuring partial crustal convection (e.g., Collins et al., 1998; François et al., 2014; Johnson et al., 2017; Moore & Webb, 2013; Van Kranendonk, 2010; Van Kranendonk et al., 2007; Wiemer et al., 2018), driven by episodic mantle plume events and gravitational instability (e.g., Fischer & Gerya, 2016; cf. Miocevich et al., 2022), although a plate tectonic origin has also been proposed (e.g., Kusky et al., 2021). The proposed model involving partial convective overturn cooling (Collins et al., 1998) predicts that the East Pilbara Terrane experienced episodic supracrustal volcanism and tonalite petrogenesis followed by quiescence during ∼10 to ∼100 million years cycles of mantle plume activities. Gravitational dripping of supracrustal rocks and buoyant rising of tonalite diapirs created the hallmark dome-and-keel geometry (Figure S1 in Supporting Information S1). Episodic magmatism and subsequent crustal convection introduced diverse deformation, metamorphism, metasomatism conditions, as well as vigorous material exchanges between the surface and mantle (e.g., Collins et al., 1998; François et al., 2014). In this model, (ultra)mafic magmatism associated with mantle plumes produces kilometer-scale ultramafic intrusions with or without fractional crystallization (e.g., Smithies et al., 2007). No subduction activity and associated tectonically-emplaced mantle rocks are predicted at crustal levels (e.g., Collins et al., 1998). Indeed, no lithology so far in the East Pilbara Terrane has been interpreted as tectonically emplaced mantle rocks (Hickman, 2021). Thus, Pilbara ultramafic rocks can be used as non-plate tectonic crustal products to compare with Isua ultramafic rocks.

3. Methods

3.1. Sampling and Data Compilation

Three ultramafic rock samples (AL52614-4A, AW52614-4A, and AW52614-6) collected from the Gap Intrusion of the East Pilbara Terrane and six samples (AW17724-1, AW17724-2C, AW17724-4, AW17725-2B, AW17725-4, and AW17806-1) collected from the Isua supracrustal belt were analyzed in this study (Figure 1). Isua samples AW17724-2C, AW17724-4 (lens B in the north), and AW17725-4 (lens A in the south) were collected from the two meta-peridotite lenses which have been previously interpreted as tectonic mantle slices (e.g., Friend & Nutman, 2011; Nutman et al., 2020). Isua sample AW17724-1 was collected from a serpentinite layer that envelopes meta-peridotite lens B. Isua sample AW17725-2B was collected from an ultramafic outcrop near the northern meta-tonalite, ∼300 m east of lens B. Isua sample AW17806-1 was collected from an ultramafic outcrop within eastern portion of the supracrustal belt, near the northern meta-tonalite body (Figure 1a, Table 1).

To test models of their petrogenesis, we compiled literature data and inspected our samples using thin-section petrography and acquisition of whole-rock major/trace element data (Table S1), spinel geochemistry (Table S2), and HSE abundances (Table S3). Compiled Isua and Pilbara data include results of previous studies focused on ultramafic rocks located adjacent to our sample locations. These outcrops include: (a) ultramafic rocks collected across the Isua supracrustal belt (including the meta-peridotite lenses) studied by Szilas et al. (2015), Friend and Nutman (2011), and Waterton et al. (2022) (Figure 1a); (b) ultramafic rocks from enclaves within the meta-tonalite located south of the Isua supracrustal belt (Van de Löcht et al., 2018, 2020); and (c) ultramafic rocks from the

Table 1
Mineralogy and Location Information of Investigated Samples

Sample ID	GPS coordinates (WGS84 datum)	Location/unit	Mineralogy
The Isua supracrustal belt			
AW17724-1	65.153681N, 50.143989W	Serpentinite layer enveloping the meta-peridotite lens B in the western belt	Serpentine + talc + magnetite
AW17724-2C	65.153974N, 50.144801W	The meta-peridotite lens B in the western belt	Olivine + serpentine + magnetite ± Ti-humite ± magnesite
AW17724-4	65.156,859N, 50.143,249W	The meta-peridotite lens B in the western belt	Serpentine + magnetite + magnesite ± talc
AW17725-2B	65.154857N, 50.138543W	~300 m east of lens B in the western belt	Carbonate + magnetite ± serpentine
AW17725-4	65.139544N, 50.149716W	The meta-peridotite lens A in the western belt	Serpentine + magnesite + olivine ± magnetite
AW17806-1	65.191627N, 49.840547W	An outcrop in the eastern belt near the north tonalite	Olivine + pyroxene + tremolite ± serpentine ± Fe-Ti-Cr oxides
The East Pilbara Terrane			
AW52614-4A	20.917983S, 119.982300E	The Gap Intrusion	Serpentine + Fe-Ti-Cr oxides + chlorite ± apatite
AL52614-4A	20.917983S, 119.982300E	The Gap Intrusion	Serpentine + Fe-Ti-Cr oxides + chlorite
AW52614-6	20.930950S, 119.867500E	The Gap Intrusion	Serpentine + Fe-Ti-Cr oxides + chlorite

Nob Well Intrusion of the East Pilbara Terrane (Geological Survey of Australia, 2013 Database, 2013; Figure 1b). Data from other ultramafic rocks that have been variably interpreted as cumulates or mantle peridotites (see the Supporting Information S1 for all references) are compiled for petrogenetic analyses. These ultramafic rocks were collected from variably deformed and altered Archean ultramafic complexes (e.g., McIntyre et al., 2019), Archean lithospheric mantle (e.g., Ishikawa et al., 2017), massive layered intrusions (e.g., Coggon et al., 2015), collisional massifs (e.g., Wang et al., 2013), and volcanic xenoliths (e.g., Ionov, 2010) or mantle rocks extracted from ocean drilling (e.g., Parkinson & Pearce, 1998). Modeled cumulates (Mallik et al., 2020) and variably depleted and refertilized mantle rocks (e.g., Chin et al., 2014, 2018) are also generated (see Section 5.4) and compiled in this study.

3.2. Analytical Details

The whole-rock major element concentrations of Pilbara ultramafic samples were analyzed in the Peter Hooper GeoAnalytical Laboratory at Washington State University in Pullman, Washington. Major elements (e.g., MgO, FeOt, and SiO_2) were analyzed using a Thermo-ARL Advant'XP + sequential X-ray fluorescence spectrometer (XRF). Sample preparation, analytical conditions, and precisions/accuracy of the analyses follow procedures detailed in Johnson et al. (1999). Whole-rock major element concentrations of Isua ultramafic samples were determined at the State Key Laboratory for Mineral Deposit Research in Nanjing University, China. Small rock fragments of Isua ultramafic samples were crushed into gravel-size chips. Clean chips were then powdered to 200 mesh for major element analyses. Measurements of whole-rock major elements were performed using a Thermo Scientific ARL 9900 XRF. The measured values of diverse rock reference materials (BHVO-2 and BCR-2) indicate that the analytical precision is better than 10% for all major elements, better than 3% for elements Si, Ti, Al, Fe, Mn, Mg, Ca, K, and P, and better than 6% for Na.

Trace element concentrations of Pilbara ultramafic samples were acquired using an Agilent 7700 inductively coupled plasma mass spectrometer (ICP-MS) in the Peter Hooper GeoAnalytical Laboratory at Washington State University. Sample preparation, analytical conditions, and precisions/accuracy of the analyses are detailed in Knaack et al. (1994). Trace element contents of Isua ultramafic samples were obtained at Nanjing Hongchuang Exploration Technology Service Company, China. About 100 g of solid samples from each Isua ultramafic sample were crushed using a corundum jaw crusher. Crushed rocks were then pulverized into fine powder using an agate ball mill. Details of sample preparation, analytical procedures, and precisions are as follows. The closed pressure acid dissolution method was used for digestion of silicate rock samples. About 50 mg of rock powder were weighed directly into a steel-jacketed, high-pressure polytetra fluoroethylene bomb and dissolved using an acid mixture of 1.5 mL of 29 mol/L HF and 1 mL of 15 mol/L HNO_3 at 190°C for 72 hr. The digested solution

was evaporated to wet salt and treated twice with 1 mL of concentrated HNO_3 to avoid the formation of fluorides. The evaporated residue was dissolved with 1.5 mL HNO_3 and 2 mL H_2O, and the Teflon bomb was resealed and placed in an oven at 190°C for 12 hr. The final solution was transferred to a polyethylene bottle and diluted to 50 mL using H_2O. Trace element analyses were performed using an Agilent 7900 ICP-MS. The total quantitative analyses of trace elements were achieved by external standard BCR-2 and BHVO-2 and internal standard Rh doped on line using an Agilent 7900 ICP-MS wet plasma. All elements were repeatedly scanned five times, which resulted in precision 1RSD better than 5%. The margin of error of all trace element results for rock powder reference materials was within 10%.

The major element compositions of spinel from the Pilbara ultramafic samples were obtained using a JEOL JXA8230 Electron Probe Microanalyser (EMPA) at the University of Leeds, United Kingdom. Major element mineral (e.g., olivine, spinel, and serpentine) compositions of the Isua ultramafic samples were analyzed in situ on petrographic thin sections using a JEOL JX8100 EMPA at the Guangzhou Institute of Geochemistry, Chinese Academy of Sciences. The EMPA analyses were performed under an accelerating voltage of 15 kV and a beam current of 20 nA. Images of the Isua ultramafic samples were collected using a Carl Zeiss SUPRA55SAPPHIR Field Emission Scanning Electron Microscope.

HSE concentrations and Re–Os isotopic data were obtained at the Institute of Geology of the Czech Academy of Sciences, Czech Republic, using the methods detailed in Topuz et al. (2018). In brief, the samples were dissolved and equilibrated with mixed ^{185}Re–^{190}Os and ^{191}Ir–^{99}Ru–^{105}Pd–^{194}Pt spikes using Carius Tubes (Shirey & Walker, 1995) and reverse aqua regia (9 mL) for at least 72 hr. Decomposition was followed by Os separation through solvent extraction by $CHCl_3$ (Cohen & Waters, 1996) and Os microdistillation (Birck et al., 1997). Ir, Ru, Pt, Pd, and Re were separated from the remaining solution using anion exchange chromatography and analyzed using a sector field ICP-MS Element 2 (Thermo) coupled with Aridus II™ (CETAC) desolvating nebulizer. The isotopic fractionation was corrected using a linear law and standard Ir, Ru, Pd, Pt (E-pond), and Re (NIST 3143) solutions that were run with samples. In-run precision of measured isotopic ratios was always better than ±0.4% (2σ). Os concentrations and isotopic ratios were obtained using negative thermal ionization mass spectrometry (Creaser et al., 1991; Völkening et al., 1991). Samples were loaded with concentrated HBr onto Pt filaments with $Ba(OH)_2$ activator, and analyzed as OsO_3^- using a Thermo Triton thermal ionization spectrometer with Faraday cups in dynamic mode, or using a secondary electron multiplier in a peak hopping mode for samples with low Os concentrations. Internal precision for $^{187}Os/^{188}Os$ determination was always equal to or better than ±0.2% (2σ). Measured Os isotopic ratios were corrected offline for oxygen isobaric interferences, spike contribution, and instrumental mass fractionation using $^{192}Os/^{188}Os = 3.08271$ (Shirey & Walker, 1998).

Fe contents of all data were recalculated to represent FeOt using the procedure in Gale et al. (2013). Results were plotted with GCDKit freeware developed by Janoušek et al. (2006).

4. Results

4.1. Petrographic Observations

We performed thin-section petrographic analysis of Isua and Pilbara ultramafic samples to observe rock microtextures and mineral assemblages that reflect igneous and alteration signatures, as these are important for geochemical interpretations of altered samples. Isua ultramafic samples show varying degrees of alteration (Figure 2 and Figure S2 in Supporting Information S1). Samples AW17724-1, AW17724-4, and AW17725-2B are dominated by serpentine, magnetite, and carbonates with the absence of olivine, pyroxene, or protolith textures (Figure 2d and Figure S2 in Supporting Information S1). On the other hand, olivine grains are preserved in three samples (i.e., AW17724-2C from lens B, AW17725-4 from lens B, and AW17806-1; Figures 2a–2c) and cross-cut or overgrown by retrograde serpentine minerals (Figure 2a). In addition to serpentinization, meta-peridotite lens samples AW17724-4C and AW17725-4 show varying degrees of carbonitization (Figures 2a and 2b), whereas sample AW17806-1 records tremolite as an alteration product (Figure 2c). Small (submicron to ~20 μm) serpentine, magnesite, and/or magnetite can be found within olivine grains as inclusions or alteration products associated with cracks/veins (Figures 2a and 2b). Relict olivine grains preserved in sample AW17725-4 show polygonal textures, but the protolith textures of AW17806-1 and AW17724-2C are altered beyond recognition (Figures 2b and 2c). Ti-humite phases only occur in AW17724-4 (Figure 2a).

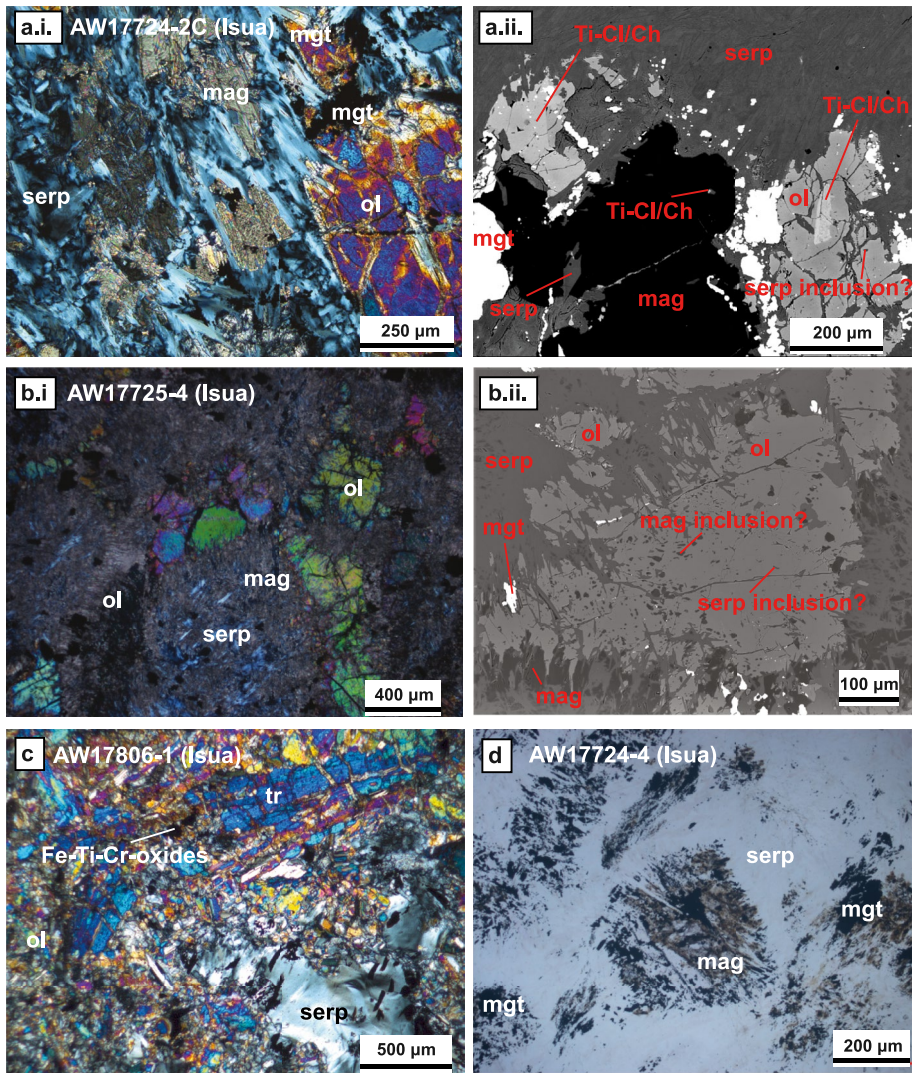

Figure 2. Representative thin section microphotographs and scanning electron microscopic images of samples from the Isua supracrustal belt. (a) Sample AW17724-2C preserves primary olivine grains (i and ii). Two generations of serpentine minerals may be present (ii): serpentine minerals forming inclusions in the olivine grains, and serpentine minerals occuring as lepidoblastic assemblages in the matrix cutting olivine, magnesite, and Ti-humite. Alternatively, there may be only one generation of serpentine minerals with those in the olivine being associated with cracks or veins not visible on this thin section plane. Due to the observed alteration, primary igneous textures of this sample cannot be identified. (b) Local preservation of polygonal textures (i) by olivine grains in sample AW17725-4. Olivine in this sample contains abundant magnesite and rare serpentine (ii), which may represent inclusions or alteration products. (c, d) Loss of most primary ultramafic silicates and rock textures of some Isua samples due to strong alteration (e.g., serpentinization and/or amphibolite facies metamorphism). Mineral abbreviations: mag: magnesite; mgt: magnetite; ol: olivine; serp: serpentine; Ti-cl: Titano-clinohumite; Ti-ch: Titano-chondrodite; tr: tremolite.

In contrast to Isua samples, Pilbara samples have experienced complete serpentinization and minor carbonitization, such that no primary ferromagnesian silicates can be identified (Figures 3a–3c and Figure S2 in Supporting Information S1). In all Pilbara samples, serpentine grains form clusters that show similar extinction. Many such clusters have quasi-equant granular outlines. We interpret these serpentine clusters to be pseudomorphs after olivine. The interstitial space between the olivine-shaped clusters is occupied by chlorite and/or Fe–Cr–Ti oxide minerals (Figures 3a and 3b) or serpentine (Figures 3a–3c). The olivine-shaped serpentine clusters appear to form self-supporting structures. Some interstitial serpentine clusters preserve two pairs of relict cleavages at ~90°, indicating a pyroxene precursor (Figure 3a). Some interstitial serpentine clusters are larger than the olivine-shaped serpentine clusters and enclose many of the latter grains, as illustrated in Figure 3c with two sets

10.1029/2022GC010519

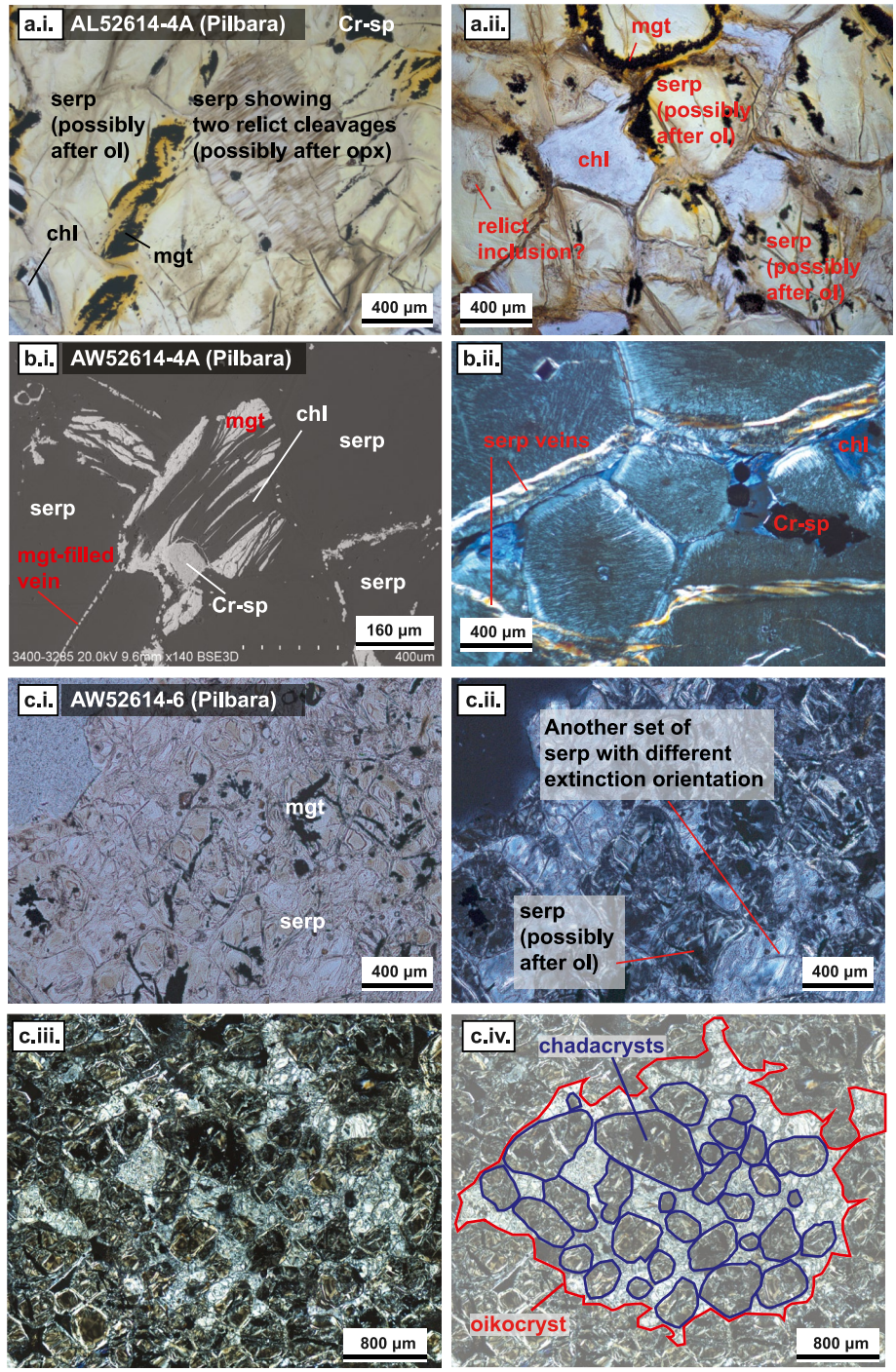

Figure 3. Representative thin section microphotographs and scanning electron microscopic images of samples from the East Pilbara Terrane. Pilbara samples show complete serpentinization, yet their primary rock textures are preserved by serpentine pseudomorphs. (a) Sample AW52614-4A shows compacted olivine-shaped serpentine clusters (ii) which locally form polygonal textures (shown by abundant 120° triple junctions). (b) Alteration minerals such as chlorite, serpentine, and magnetite occur in interstitial spaces (i) and veins in sample AW52614-4A (ii). In (c.ii–civ), two sets of serpentine clusters are recognized with the cross-polarized light photomicrographs. One set shows black/dark gray colors with outlines similar to olivine grains. Another set is white/light gray and appears to enclose the serpentine clusters of the first set. This texture resembles cumulate textures, wherein smaller chadacrysts could be included in larger oikocrysts. Mineral abbreviations: chl: chlorite; Cr-sp: Cr-spinel; mag: magnesite; mgt: magnetite; ol: olivine; opx: orthopyroxene; serp: serpentine.

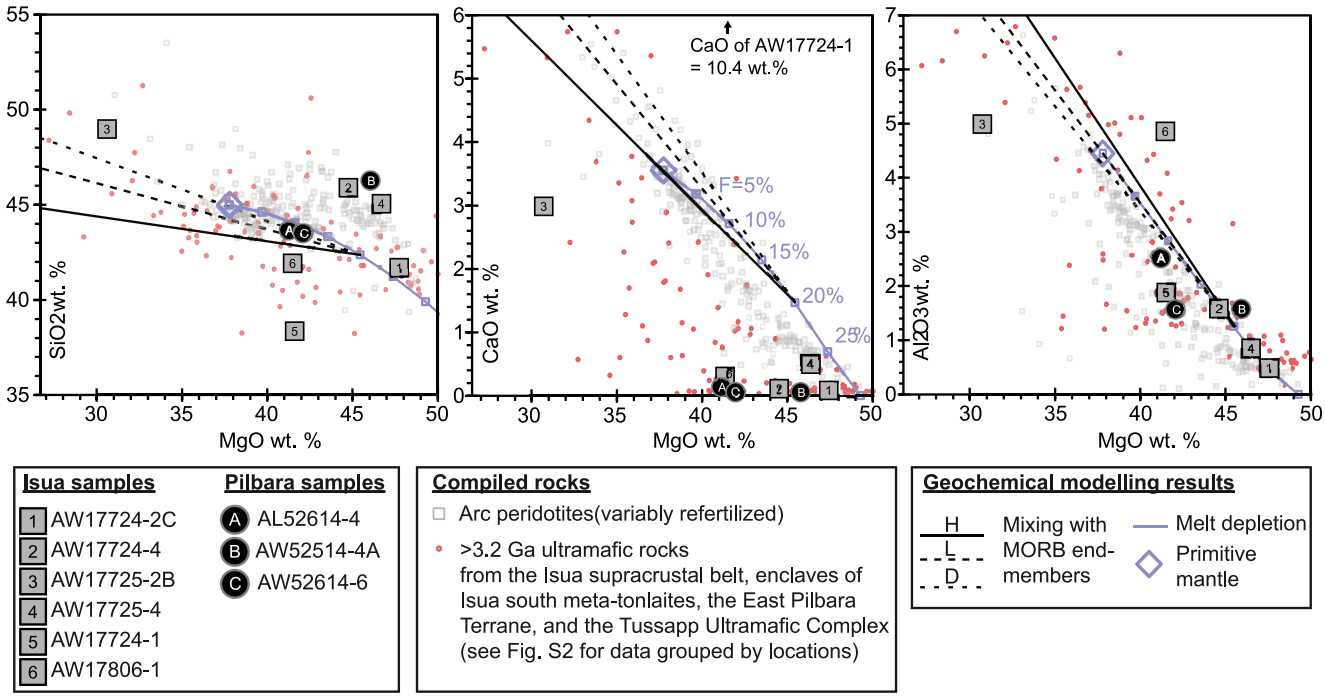

Figure 4. Major element abundances versus Mg# of Pilbara and Isua ultramafic samples. Geochemistry of arc peridotites, other compiled >3.2 Ga ultramafic rocks from the Isua and Pilbara areas, and MELTS modeling results (compiled from Chin et al., 2014) are also plotted for comparison. References of compiled >3.2-Ga ultramafic rocks are listed in the Figure 1 caption. All data are presented using anhydrous values (i.e., all major element abundances are normalized to zero loss-on-ignition and 100 wt.% total). Primitive mantle values are from McDonough and Sun (1995). The mixing lines represent mixing between 20% depleted primitive and mid-ocean ridge basalt end-members H, L, and D (Elthon, 1992), which are representative of variably altered arc peridotites (Chin et al., 2014). See Figure S4 in Supporting Information S1 caption for data sources.

of serpentine clusters via different brightnesses due to extinction. Such patterns resemble poikilitic textures in which early-formed chadacrysts are surrounded by younger, large oikocrysts (Johannsen, 1931). In some locations, olivine-shaped serpentine clusters are compacted, forming polygonal textures (Figure 3c). Late-stage alteration veins/cracks can be seen in samples AW52514-4A and AL52614-4A (Figure 3b).

4.2. Whole-Rock Major and Trace Element Characteristics

Whole-rock major and trace element characteristics are often used to indicate the petrogenetic conditions, such as the degree of melt depletion and the sources of ultramafic rocks (e.g., Niu & Hekinian, 1997; Van de Löcht et al., 2020), although effects of alteration (as observed in Section 4.1) must be considered. Isua ultramafic rocks have SiO_2 of ~38–49 wt.%, MgO of ~31–47 wt.%, CaO of ~0.03–10.49 wt.%, Al_2O_3 of ~0.5–5.0 wt.%, FeOt of ~6.2–10.7 wt.%, Mg# (that is, Mg/(Mg + Fe)) of 84–93, Cr of ~840–6,910 ppm, Ni of ~1,900–3,680 ppm, and loss-on-ignition (LOI) of ~5–21 wt.% (all major oxide concentrations are anhydrous values, i.e., normalized to zero LOI and 100 wt.% total; Figures 4 and 5, Figures S3–S4 in Supporting Information S1 and Table S1). Trace element abundances of Isua ultramafic rocks are mostly 0.1–10 times those inferred for the primitive mantle (McDonough & Sun, 1995; same below; Figure 6). These ultramafic rocks have unfractionated to mildly fractionated ($[La/Sm]_{PM}$ of ~1.1–3.8) light to medium rare earth elements (LREE to MREE) and heavy rare earth elements (HREE) ($[Gd/Yb]_{PM}$ of ~0.3–1.6) (Figures 6a and 6c). Th concentrations and Gd/Yb ratios (proxies for alterations; Figure 6b; Deschamps et al., 2013) range from 0.04 to 1.13 ppm and 0.4–2.1, respectively. Some Isua ultramafic samples show negative Nb anomalies. Both positive and negative Eu anomalies are observed (Figure 6c).

Pilbara ultramafic rocks have whole-rock SiO_2 of ~43–46 wt.%, MgO of ~41–45 wt.%, CaO of 0.02–0.12 wt.%, Al_2O_3 of ~1.6–2.5 wt.%, FeOt of ~6.1–12.8 wt.%, Mg# of 85–93, Cr of ~3,720–7970 ppm, Ni of 1,350–1,800 ppm, and LOI of 12.3–12.9 wt.% (Figures 4 and 5, Figures S3 and S4 in Supporting Information S1, Table S1). Trace element abundances in these samples are 0.1–10 times those of primitive mantle. Pilbara samples show mildly

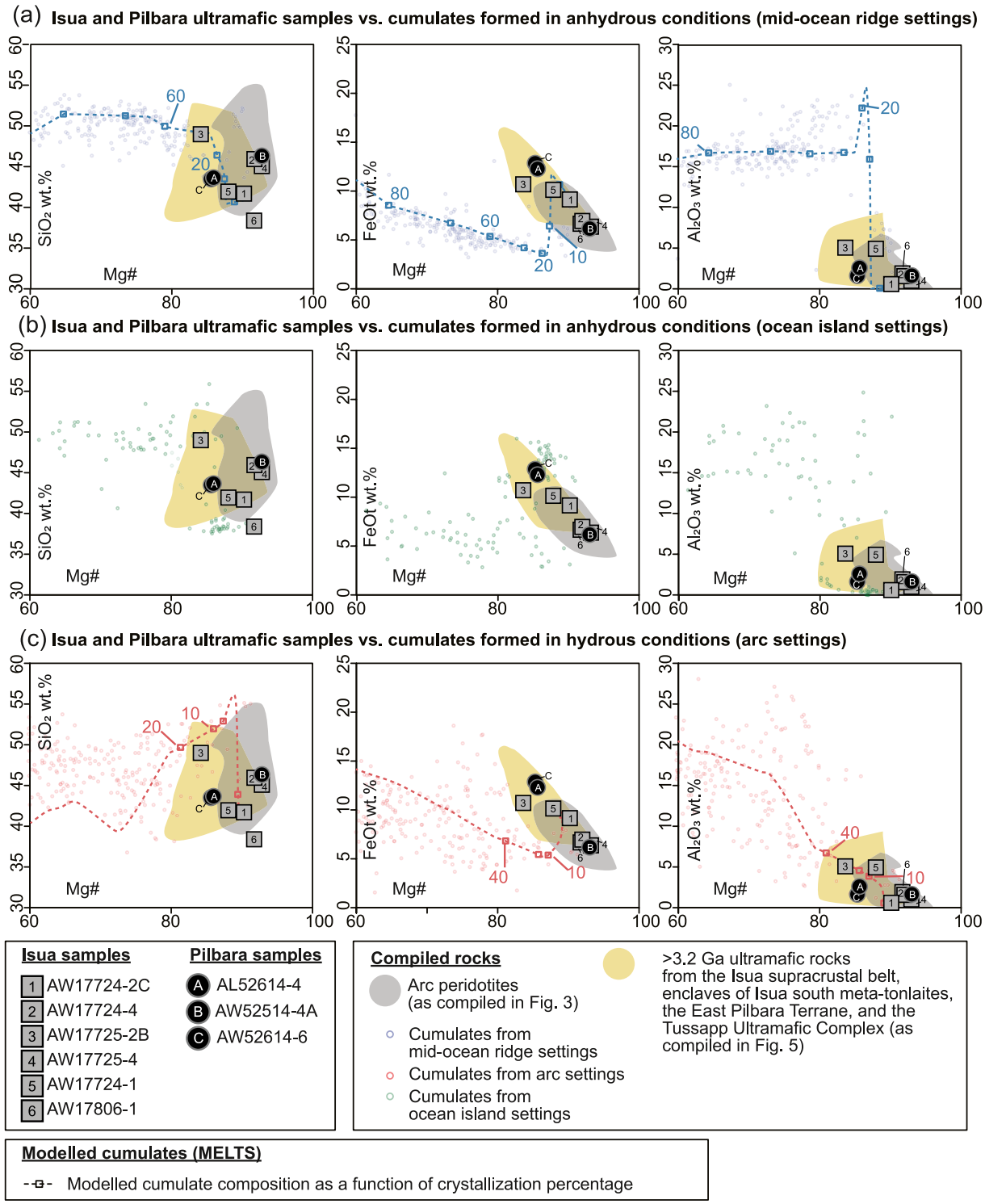

Figure 5. Major element geochemical characteristics of the Isua and Pilbara ultramafic samples in comparison with those of Phanerozoic cumulates, arc peridotites, >3.2 Ga ultramafic rocks (see Figure S4 in Supporting Information S1 for data sources), and modeled cumulate composition as a function of crystallization percentage. All data are presented using anhydrous values (i.e., all major element abundances are normalized to zero loss-on-ignition and 100 wt.% total). The data in this figure show that Isua and Pilbara ultramafic rocks, Mg-rich cumulates and mantle peridotites have similar major element geochemical systematics. Data sources for the cumulates and MELTS modeling curves are from Chin et al. (2018), Mallik et al. (2020), and references therein. Specifically, cumulates from oceanic island settings (panel b) cannot be modeled due to limitations of MELTs programs on modeling ultrahigh pressure (>3 GPa) melting and enriched mantle sources, which are necessary for generating oceanic island basalts.

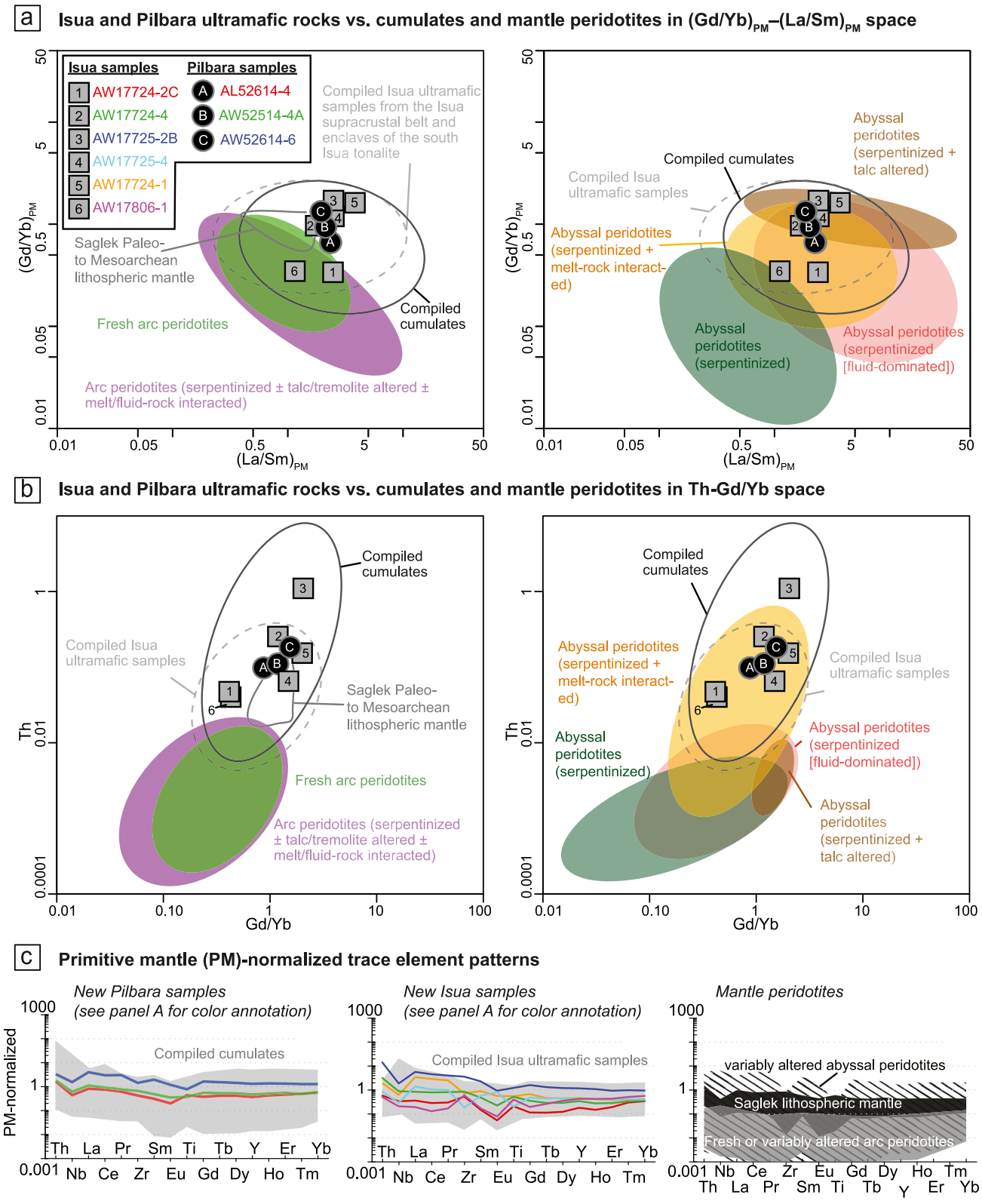

Figure 6.

fractionated LREE to HREE ($[La/Sm]_{PM}$ of 1.9–2.4) and generally flat HREE trends ($[Gd/Yb]_{PM}$ of 0.8–1.1) (Figure 6). Th concentrations and Gd/Yb ratios of Pilbara ultramafic samples range from 0.10 to 0.19 ppm and 1.2–1.7, respectively. These samples have weak negative Nb anomalies and negative Eu anomalies (Figure 6b).

4.3. HSE Characteristics

The primitive mantle-normalized (Becker et al., 2006) HSE patterns of the Pilbara samples exhibit similar fractionated patterns characterized by strong Ru enrichment over Os–Ir ($(Ru/Ir)_{PM}$ = 2.0–3.5) and Pt depletion over Os-Ir ($(Pt/Ir)_{PM}$ = 0.3–0.6), whereas Pd and Re contents are highly variable (Figure 7). One Pilbara sample (AW52514-4A) shows significantly higher Pd abundance (close to the primitive mantle value) compared to the rest of the samples. The present-day $^{187}Os/^{188}Os$ values range between ∼0.1094 and 0.1166. Re contents are high in two samples (0.13 ppb in sample AL52614 and 0.35 ppb in sample AW52514), resulting in superchondritic $^{187}Re/^{188}Os$ (0.53 and 0.86, respectively) and unrealisticly low initial $^{187}Os/^{188}Os$ values (<0.078) calculated at ∼3.4 Ga.

4.4. Mineral Geochemistry

Olivine grains in Isua sample AW17724-2C (lens B) have extraordinarily high Mg# values of ∼95–98 and NiO of ∼0.39–0.63 wt.%. In contrast, olivine grains in Isua sample AW17725-4 (lens A) have Mg# values of ∼87 and NiO of ∼0.52–0.61 wt.% (Table S2). Ti-humite phases in sample AW17724-2C have variable TiO_2 abundances of ∼3.0–8.1 wt.%. All analyzed spinel grains in the Isua samples contain a high magnetite component (i.e., FeOt of ∼90 wt.%) (Table S2).

Spinel of both chromite and magnetite compositions occur in the Pilbara samples. Specifically, chromite spinel grains have Cr_2O_3 of ∼40–50 wt.%, TiO_2 of 0.6–4.3 wt.%, and MgO of 5–12 wt.%. The Cr# (Cr/(Cr + Al)) values and Mg# values of chromite spinel grains are ∼65–75 and ∼17–46, respectively (Figure 8; Table S2).

5. Discussion

Our new petrological and geochemical data for six ultramafic samples from the Isua supracrustal belt and three ultramafic samples from the East Pilbara Terrane show that: (a) Isua and Pilbara samples have been variably altered and contain several kinds of alteration minerals (e.g., serpentine, carbonate, and/or ti-humite) that replaced igneous ferromagnesian silicates (Figures 2 and 3); (b) Pilbara ultramafic samples preserve poikilitic textures and polygonal textures (Figure 3); one Isua sample (AW17725-4 from lens A) also preserves relict polygonal textures (Figure 2b); (c) trace element abundances in Isua and Pilbara ultramafic samples are generally 0.1 to 10 times of the primitive mantle values (Figure 6c); (d) two out of three Pilbara ultramafic samples show fractionated, relatively high concentrations of Os and Ir versus Pt, Pd, and Re (Figure 7d), which are similar to some Isua meta-peridotite lens samples (Waterton et al., 2022); and (e) chromite spinel in Pilbara ultramafic samples feature Cr# of ∼65–75 and Mg# of ∼17–46 (Figure 8). In the following sections, we first discuss the potential impacts of alterations on petrology and geochemistry. Then, we show that new and existing petrography, geochemistry, and microstructures of Isua and Pilbara ultramafic rocks are consistent with a crustal cumulate origin, whereas an origin as thrust-emplaced mantle slices is not consistent with observed geochemistry. We then discuss the implications for testing early Earth tectonic models and the initiation of plate tectonics.

Figure 6. Trace element characteristics for Isua and Pilbara ultramafic samples in comparison with compiled cumulates and variably altered mantle peridotites. (a) Primitive mantle normalized Gd/Yb and La/Sm ratios (i.e., $(Gd/Yb)_{PM}$ and $(La/Sm)_{PM}$) of samples from this study and literature. (b) Th and Gd/Yb ratios of investigated samples and compiled rocks. (c) Primitive mantle-normalized spider diagrams showing trace element patterns of samples from this study and literature (see Figure S6 in Supporting Information S1 for spider diagrams grouped by sample locations). These diagrams show that new and compiled data for ultramafic rocks from the Isua supracrustal belt have similar trace element characteristics to meta-peridotite enclaves from the south Isua meta-tonalites, Pilbara ultramafic samples, and other Eoarchean ultramafic cumulates. Only some abyssal peridotites and lithospheric mantle peridotites which experienced serpentinization and melt-rock interactions have comparable trace element patterns. Other mantle peridotites have lower Th, Gd/Yb, $(Gd/Yb)_{PM}$, and/or $(La/Sm)_{PM}$ values. See Figure S6 in Supporting Information S1 caption for references of compiled data. Primitive mantle values are from McDonough and Sun (1995).

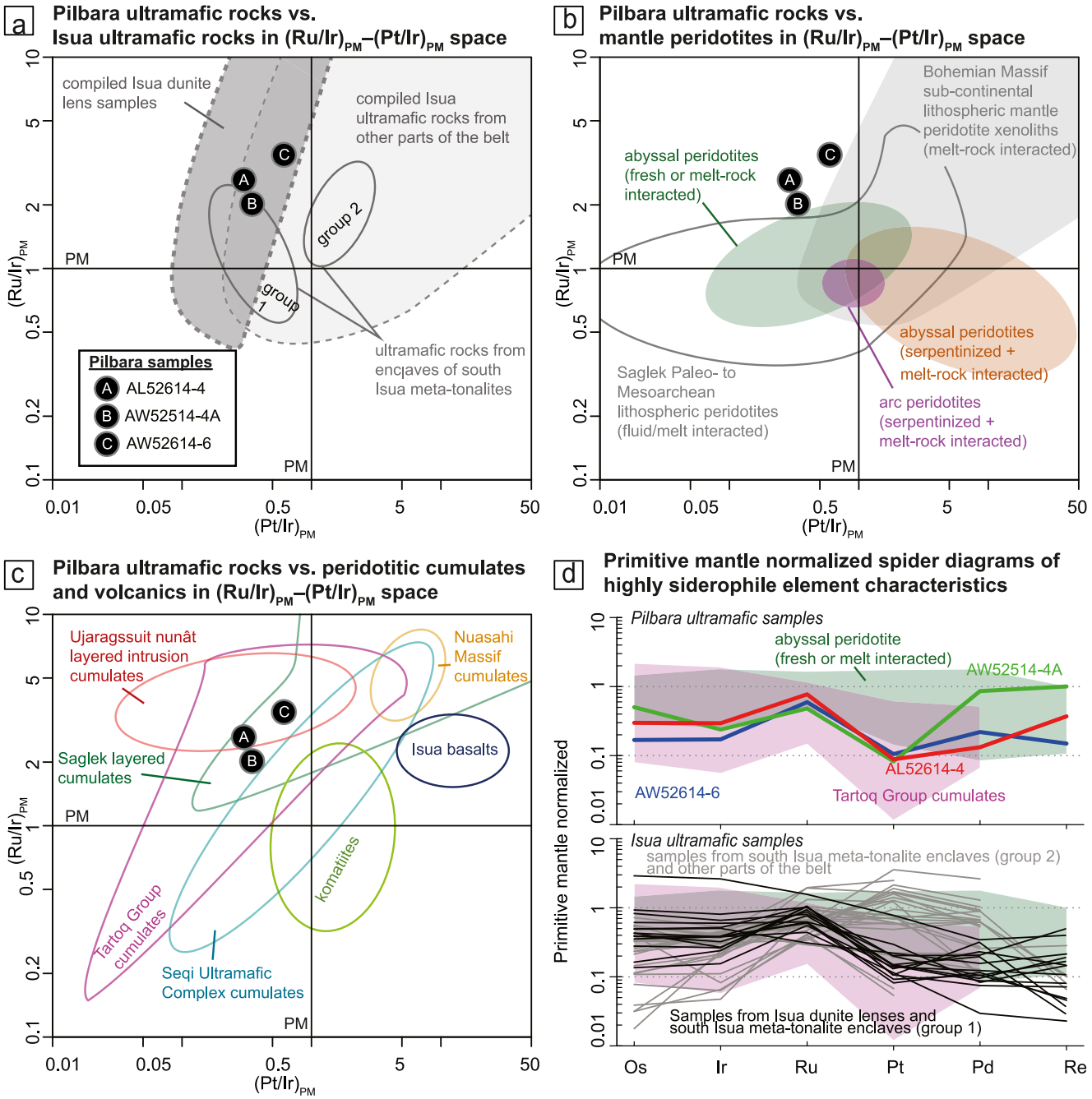

Figure 7. Highly siderophile element (HSE) (including platinum-group elements, PGEs: Os, Ir, Ru, Pt, and Pd) characteristics of the Pilbara samples, Isua ultramafic rocks, cumulates, volcanics, and mantle peridotites. Panels (a–c) show primitive mantle (PM)-normalized Pt/Ir and Ru/Ir ratios (i.e., $(Pt/Ir)_{PM}$ and $(Ru/Ir)_{PM}$) of new Pilbara samples in comparison with those of Isua ultramafic rocks (from the supracrustal belt and peridotite enclaves, see Figure 4 caption; panel a), mantle peridotites (panel b), volcanics (komatiites and basalts) and peridotitic cumulates (panel c). Peridotites from meta-tonalite enclaves south of the Isua supracrustal belt are divided by Van de Löcht et al. (2018) into two groups according to their HSE signatures: "group 2" peridotites have higher Pt, Pd, and Re versus "group 1" peridotites. Panel d shows primitive mantle-normalized HSE patterns of new Pilbara samples and representative compiled rocks (see Figure S7 in Supporting Information S1 for HSE patterns of all new and compiled rocks). These plots show that the HSE characteristics of Pilbara ultramafic rocks are similar to those of cumulate rocks, but are different from those of mantle peridotites. Furthermore, HSE patterns of ultramafic rocks from peridotite enclaves of meta-tonalites south of the Isua supracrustal belt are consistent with those of cumulates and do not require mantle peridotite origins (cf. Van de Löcht et al., 2018). Data sources can be found in the Figure S7 in Supporting Information S1 caption. Primitive mantle values are from Becker et al. (2006).

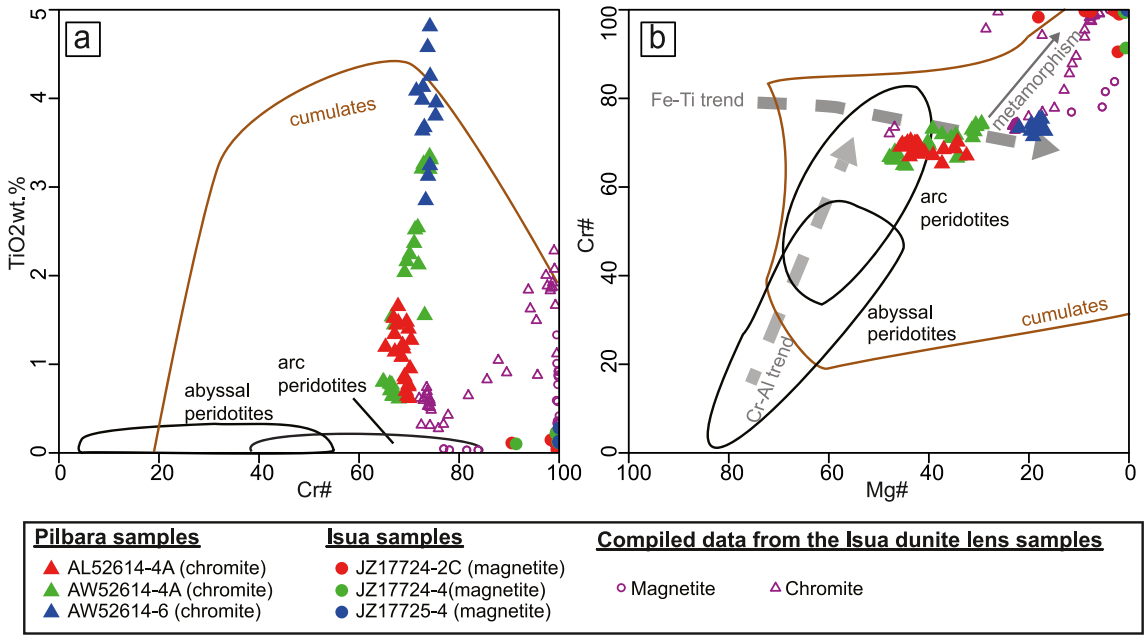

Figure 8. Geochemical signatures of spinel in Pilbara and Isua samples, plotted with compiled fields for ultramafic cumulates and mantle peridotites. Panel a shows Cr# values (Cr/(Cr + Al)) and TiO_2 concentrations of spinel. Panel b shows Mg# (Mg/(Mg + Fe)) and Cr# values of spinel. The Fe–Ti trend of spinel (representing equilibration during fractional crystallization) and Cr–Al trend of spinel (representing equilibration in mantle) are plotted for comparison. These plots indicate that spinel from Isua and Pilbara samples are similar to those of cumulates, but are different from those of mantle peridotites. Compiled spinel from Isua ultramafic rocks is from Szilas et al. (2015). The spinel field of the cumulates is fit by spinel data for the Uralian-Alaskan type intrusions (Abdallah et al., 2019; Garuti et al., 2003; Himmelberg & Loney, 1995; Krause et al., 2011; Thakurta et al., 2008), Mesoarchean Seqi Ultramafic Complex of southwestern Greenland (Szilas et al., 2018) and data compiled in Barnes and Roeder (2001). The spinel field of arc peridotites is fit by spinel data in Ionov (2010), Parkinson and Pearce (1998), and Tamura and Arai (2006). The spinel field of abyssal peridotites is fitted by spinel data in Khedr et al. (2014), Standish et al. (2002), and Tamura and Arai (2006). Spinel Fe–Tl, Cr–Al, and metamorphic trends are from Barnes and Roeder (2001).

5.1. Assessment of Alteration Impacts

High-grade (e.g., granulite facies) metamorphism can lead to partial melting of crustal materials. These melts could strongly disturb the geochemistry and mineral assemblages of affected ultramafic rocks. However, the Isua supracrustal belt and the supracrustal rocks in the East Pilbara Terrane (Figure 1) have only experienced metamorphism as high as amphibolite facies conditions (e.g., Hickman, 2021; Ramírez-Salazar et al., 2021, 2022).

Fluid-assisted alteration could result in changes in mineral assemblages and whole-rock/mineral element concentrations including REEs, but the impacts on fluid-mobile elements (e.g., K, Ca, Si, Rb, Ba, and Sr, etc.) would be most significant (e.g., Deschamps et al., 2013; Malvoisin, 2015; Paulick et al., 2006). Some HSEs like Os, Ir, Ru, and Pt are relatively immobile during fluid-assisted alterations, but Pd and Re could be relatively mobile (e.g., Barnes & Liu, 2012; Büchl et al., 2002; Deschamps et al., 2013; Gannoun et al., 2016). Spinel Al can be increased, and Cr can be reduced during fluid-rock interactions (e.g., El Dien et al., 2019).

Melt-rock interaction is commonly observed in mantle rocks (e.g., Ackerman et al., 2009; Büchl et al., 2002; Deschamps et al., 2013; Niu, 2004; Paulick et al., 2006) where ascending melts react with wall rocks. This process is similar to reactions between cumulate phases and trapped/evolving melts during crystallization or post-cumulus processes (e.g., Borghini & Rampone, 2007; Goodrich et al., 2001; Wager & Brown, 1967). In general, melt-rock interaction can alter the geochemistry of affected rocks towards those of melts at increasing melt/rock ratios (e.g., Kelemen et al., 1992; Paulick et al., 2006). For peridotites interacting with basalts or more evolved melts, the elevation of elements that are relatively enriched in melts (e.g., Si, Ca, Th, Al, Fe, Ti, REEs, Pt, Pd, and Re) is significant (Figures 4–7; e.g., Deschamps et al., 2013; Hanghøj et al., 2010). Other effects include changes in mineral modes and/or mineral geochemistry (e.g., olivine Mg# reduction; spinel Cr-loss and Al-gain) (e.g., El Dien et al., 2019; Niu & Hekinian, 1997).

Moderate to high LOI contents (~5–21 wt.%; Figure S3a in Supporting Information S1) and the presence of serpentine, talc, and/or magnesite (Figures 2 and 3, Figure S2 in Supporting Information S1) in Isua and Pilbara

ultramafic samples show that these rocks have experienced variable degrees of serpentinization, carbonitization, and/or talc-alteration. Major element geochemistry of Isua and Pilbara ultramafic samples is similar to the serpentine mineral compositions, suggesting that serpentinization was the dominant process (Figure S3a in Supporting Information S1). Nonetheless, the potential MgO and SiO_2 loss/gain due to serpentinization may be smaller than 5 wt.% for all Isua and Pilbara samples except for Isua samples AW17725-2B and AW17806-1 (Figure S3b in Supporting Information S1). These two samples show strongly disturbed MgO and SiO_2 as well as significantly enriched Al_2O_3, which cannot be solely accounted for by serpentinization but may be related to melt-rock interactions (see below). Effects of other alterations on major element concentrations and LOI (e.g., Deschamps et al., 2013; Paulick et al., 2006) in most samples appear to be minor with the exception of sample AW17724-1, which has a high anhydrous CaO concentration (10.4 wt.%). Elevation of CaO in Isua ultramafic rocks has been interpreted as recording calcite addition during carbonitization (Waterton et al., 2022).

The similarity between pritmitive mantle-normalized trace element patterns for Isua ultramafic rocks and their nearby mafic lavas and the relatively high Th and LREE concentrations compared to those of modeled cumulates or fresh mantle residues have been explained by melt-rock interactions with co-genetic mafic melts (e.g., Friend & Nutman, 2011; Nutman, Scicchitano, et al., 2021; Szilas et al., 2015; Waterton et al., 2022). Nonetheless, there is no consensus regarding the origin of the ultramafic rocks (i.e., cumulates vs. mantle residues) or melts (i.e., non-arc lavas vs. arc lavas). Pilbara ultramafic rocks also have relatively elevated Th and LREEs and geochemical trends similar to those of local mafic lavas (Figure 6; Smithies et al., 2007). Therefore, these ultramafic rocks could also have experienced melt-rock interactions.

In summary, fluid/melt rock interaction might in part control the observed geochemistry and petrology of studied Isua and Pilbara samples. Thus, for petrogenetic interpretations, we compare the observed geochemistry and petrology of Isua and Pilbara ultramafic samples with those of cumulates and mantle peridotites that potentially experienced similar alterations including serpentinization, carbonitization, talc/tremolite alteration, and melt-rock interaction.

5.2. How Similar Could Olivine-Rich Cumulate and Mantle Peridotite Be?

Ultramafic rocks from the East Pilbara Terrane are generally interpreted as cumulates or high-Mg volcanic flows (Smithies et al., 2007). Our Pilbara ultramafic samples show poikilitic textures (Figure 3c) as preserved by the serpentine pseudomorphs, which can only be explained through the formation of olivine-rich cumulates (Wager & Brown, 1967). Notably, some features of our Pilbara ultramafic samples and other compiled cumulates are similar to signatures used to support mantle peridotite origins for the Isua ultramafic rocks. Below, we list these features that cannot unequivocally distinguish mantle peridotites from olivine-rich cumulates and thus, cannot be useful for model testing.

Based on petrography (Figures 2 and 3), Pilbara ultramafic rocks have potentially similar protolith mineral assemblages (olivine + spinel ± pyroxene) to tectonically-emplaced, depleted mantle peridotites (e.g., Ionov, 2010), as well as Isua ultramafic rocks (this study; Szilas et al., 2015; Van de Löcht et al., 2018). Some Pilbara ultramafic rocks preserve polygonal textures of Pilbara ultramafic rocks (Figure 3b) likely developed via re-equilibration and recrystallization of cumulate olivine grains under crustal conditions (e.g., Hunter, 1996). Such textures are identified in one sample (AW17725-4) from the meta-peridotite lens (Figure 2b) and rocks sampled from nearby outcrops (e.g., Nutman et al., 1996). Evidence from the Pilbara ultramafic rocks shows that relict polygonal textures in Isua lens A samples could also result from mineral re-equilibration and recrystallization under crustal conditions (Hunter, 1996) rather than under mantle conditions (Nutman et al., 1996).

Pilbara ultramafic samples, as well as many olivine-rich cumulates, show strikingly similar whole-rock major (e.g., MgO vs. SiO_2, CaO, Al_2O_3, Cr, and Ni systematics) and non-HSE trace element geochemistry compared to some mantle peridotites and Isua ultramafic rocks (Figures 4–7 and Figures S3–S6 in Supporting Information S1). The high Th (generally >0.04 ppm), fractionated LREE trends (with $(La/Sm)_{PM}$ of ~1.9–2.4), and generally unfractionated heavy REE trends (with $(Gd/Yb)_{PM}$ of ~0.8–1.2) of Pilbara ultramafic rocks are particularly similar to melt-modified mantle peridotites from modern plate tectonic settings (e.g., Paulick et al., 2006) and Paleo- to Mesoarchean lithospheric mantle of the Slave Craton, Canada (Ishikawa et al., 2017). In comparison, fresh or fluid-altered arc and abyssal peridotites either show significantly lower Th concentrations (generally <0.01 ppm) and/or more fractionated heavy REE as evident by lower $(Gd/Yb)_{PM}$ and Gd/Yb ratios (Figure 6).

Pilbara ultramafic rocks and some Eo- or Mesoarchean cumulates from southwestern Greenland (McIntyre et al., 2019; Szilas et al., 2014, 2018) show relative depletion in Pt and Pd versus Ir and Ru, as evident by $(Pt/Ir)_{PM}$ ratios of ∼0.3–0.6 (Pilbara) and ∼0.02–5 (complied cumulates) (Figure 7). This feature is commonly interpreted to represent melt depletion in mantle (e.g., Wang et al., 2013), which was used to explain the formation of "group 1" peridotites from the enclaves of meta-tonalites, south of the Isua supracrustal belt (which have $[Pt/Ir]_{PM}$ of ∼0.2 to ∼0.5; Van de Löcht et al., 2018). However, similarly fractionated HSE patterns could be obtained by cumulates via fractional crystallization of olivine and HSE-rich alloys (e.g., Coggon et al., 2015; McIntyre et al., 2019). Therefore, the relative depletion in Pt and Pd versus Ir and Ru may be consistent with cumulate origins and not exclusive to depleted mantle rocks (Figure 7 and Figure S7 in Supporting Information S1).

Complementary to our serpentinized Pilbara sample set showing that cumulates and depleted mantle rocks could have similar bulk magmatic mineral assemblages and whole rock geochemistry, findings from modeling and other crustal ultramafic rocks indicate that they could also have similar olivine deformation fabrics and magmatic/metamorphic features.

Clinopyroxene inclusions in olivine of Isua ultramafic samples have been interpreted to reflect melt-rock interactions in the mantle (Nutman, Scicchitano, et al., 2021). We argue that clinopyroxene undersaturation and olivine saturation are possible across a range of pressure-temperature-composition combinations (Chen & Zhang, 2009 and references therein) and could occur under crustal conditions during magma crystallization in the presence of water, crustal assimilation, and/or magma recharge (e.g., Gordeychik et al., 2018; Kelemen, 1990).

Although the B-type olivine fabrics (Kaczmarek et al., 2016) have been interpreted to reflect mantle environments, the fabrics are also consistent with crustal cumulate origins (also see Waterton et al., 2022) because such fabrics can form via processes that could happen at crustal levels (e.g., Chin et al., 2020; Holtzman et al., 2003; Nagaya et al., 2014; Yao et al., 2019). Specifically, olivines with B-type fabrics can form via deformation in the presence of melts (e.g., Chin et al., 2020; Holtzman et al., 2003); via compaction during cumulate formation (e.g., Yao et al., 2019); and via dehydration breakdown of oriented antigorite crystals (Nagaya et al., 2014). Therefore, B-type olivine fabrics do not represent a diagnostic signature of deformation in the mantle wedge (cf. Kaczmarek et al., 2016). We argue that with current geochemical and mineral textural data from Isua ultramafic rocks, mantle wedge conditions are not required, and cumulate origins are viable.

Finally, the presence of Ti-humite in Isua ultramafic rocks has been interpreted to reflect low-temperature, UHP (i.e., <500°C, >2.6 GPa) metamorphism (Friend & Nutman, 2011; Guotana et al., 2022; Nutman et al., 2020) primarily using the petrogenetic grid generated from experiments (i.e., Shen et al., 2015). However, the results of Shen et al. (2015) cannot be directly applied to Isua ultramafic rocks. This is because Shen et al. (2015) experimented on a CO_2-free chemical system, but Isua ultramafic rocks preserve carbonate phases (Figure 2a) that appear to be a reaction product of an olivine-breakdown reaction, equally producing antigorite and Ti-humite (Ramírez-Salazar et al., 2022). It is possible that Ti-humite could have been formed under much lower pressures, such as amphibolite-facies conditions recorded by the other parts of the Isua supracrustal belt (Ramírez-Salazar et al., 2021; Waterton et al., 2022). Therefore, the Isua supracrustal belt may not have experienced (U)HP metamorphism, obviating the need for plate tectonic subduction (Waterton et al., 2022; cf. Friend & Nutman, 2011; Guotana et al., 2022; Nutman et al., 2020).

In summary, findings from Pilbara ultramafic samples and other works show that variably altered, olivine-rich crustal cumulates and depleted mantle rocks could be similar in terms of mineral assemblages, rock textures, and whole-rock major and trace element geochemistry. In the case of Isua ultramafic rocks, distinguishing their origins is complicated by extensive alterations and deformation. We argue that thus far, no features preserved in Isua ultramafic rocks can be exclusively interpreted as representing tectonically-emplaced depleted mantle rocks (cf. Nutman et al., 2020, Nutman, Scicchitano, et al., 2021; Van de Löcht et al., 2018, 2020). Instead, evidence presented below indicates that these rocks are not depleted mantle slices, but rather crustal cumulates.

5.3. Spinel Geochemistry of Isua and Pilbara Ultramafic Rocks Are Not Consistent With Depleted Mantle Rocks

Geochemistry of primary chromite grains of Isua and Pilbara ultramafic samples indicates equilibrium during magma crystallization rather than equilibrium with mantle olivine before metamorphic overprints. New and compiled and Pilbara chromite grains match the Fe–Ti trend in Mg#–Cr# space (Figure 8b). Such a trend can be

produced by equilibration of spinel phases during fractional crystallization (Barnes & Roeder, 2001) and thus, can be found in cumulates (Figure 8b). Chromite crystals of Isua and Pilbara samples also have variable TiO_2 (up to ~2 and ~5 wt.%, respectively). In contrast, due to equilibration with olivine, mantle spinel typically has high Mg# and varied Cr# (i.e., the Cr–Al trend in Figure 8b, Barnes & Roeder, 2001) as well as low TiO_2 (typically <1 wt.%; Figure 8a) (e.g., Tamura & Arai, 2006). Although fluid/melt assisted alterations could impact chromite geochemistry in mantle rocks, expected changes include Cr# reduction and Mg# increase along with the Cr–Al trend (El Dien et al., 2019), which are not consistent with the observed spinel geochemistry.

5.4. REE-HSE Signatures of Isua and Pilbara Ultramafic Rocks Are Not Consistent With Metasomatised Mantle Residues

Geochemical patterns of Isua and Pilbara ultramafic rocks indicate significant melt-rock interactions (see above). Previous studies interpreted that Isua meta-peridotites from lenses A and B are sub-arc mantle residues that interacted with co-existing arc basalt magmas (Friend & Nutman, 2011), whereas those from the southern meta-tonalite enclaves are mantle residues that interacted with adakitic slab melts (Van de Löcht et al., 2020). Below, we show that these interpretations cannot explain the HSE patterns obtained for Isua and Pilbara ultramafic rocks. Instead, the REE-HSE patterns of these ultramafic rocks reflect olivine-rich cumulates interacted with co-existing melts from crustal magma chambers or deep, potentially reduced mantle. Therefore, no ultramafic protoliths nor melt components require plate tectonic subduction at Isua and Pilbara.

Mantle residues metasomatised by slab melts have radiogenic Os isotopic signatures inherited from recycled crustal materials (Brandon et al., 1996; Gannoun et al., 2016). However, Isua and Pilbara ultramafic rocks collectively exhibit unradiogenic Os isotopic signatures (Van de Löcht et al., 2018; Waterton et al., 2022; this study). Therefore, Isua and Pilbara ultramafic rocks cannot be explained by melt-rock interactions involving slab melts (cf. Van de Löcht et al., 2020).

To reproduce REE patterns of Isua and Pilbara ultramafic rocks in the context of mantle residue origins, mixing between mantle residues (see Supporting Information S1 for details on modeling) and up to ~20% co-existing basaltic melts would be required (Figure 9a). However, such mixing proportions would significantly impact the HSE concentrations of metasomatised ultramafic rocks (Figure 9a). This is because basaltic magmas, in comparison to mantle rocks, typically have fractionated HSE patterns characterized by the enrichment of Pt–Pd and Re with respect to IPGE (e.g., Bockrath et al., 2004; Brenan et al., 2016; Fiorentini et al., 2010). For example, the limited HSE data for Isua tholeiitic basalts yield Pt and Pd abundances of ~11 and ~6 ppb, respectively (Figure 9a; Szilas et al., 2015). Thus, plausible mixing with such melts cannot generate low Pt and Pt contents preserved in Isua and Pilbara ultramafic rocks (Figure 9a).

The observed signatures of the Isua and Pilbara ultramafic rocks predict that interacted melt must contain relatively high REE and low Pt and Pd contents (both compared to primitive mantle). Below, we list several possible explanations.

Sulphide removal during magma crystallization (e.g., Lightfoot & Keays, 2005) is a mechanism that can lower the Pt and Pd abundances of the co-genetic melts. In Isua and Pilbara, some meta-basalt layers were found to contain sulphide minerals which crystallized coevally with the basalts (Appel, 1979; Hickman, 2021). Therefore, at least some Isua and Pilbara basalts may have undergone sulphide exhaustion that would lead to low HSE concentrations in the remaining melt (see Figure 9b for low HSE contents of basalts after sulphide removal; Lightfoot & Keays, 2005; Wooden et al., 1993). It is important to note that sulphide removal from basaltic melts is restricted to crustal levels (e.g., Arndt et al., 2005) and therefore, mantle residues cannot interact with such low HSE melts.

Low HSE melts can also be generated due to retention of HSE-rich phases (sulphide and/or PGE-bearing alloys) in the mantle residues after melting (e.g., Fiorentini et al., 2011; Waterton et al., 2021). Whereas there are several possibilities how to retain sulphide or PGE-bearing alloy as melt residues, none of the possibilities are consistent with partial melting in an Eoarchean mantle wedge. First, sulphur is less soluble in melts under higher pressures (O'Neill & Mavrogenes, 2002), whereas mantle-derived HSE-poor melts indicate deep mantle sources (e.g., low HSE komatiites; Fiorentini et al., 2011). Second, Pd might become compatible in majoritic garnets, and PGE-alloys might be stable in the deep mantle (e.g., >7 GPa; Waterton et al., 2021 and references therein). Third, PGE-alloys can be stable under reduced mantle conditions even during high-degree partial melting (e.g., Fiorentini et al., 2011). Therefore, the potential presence of low Pt and Pd Isua tholeiitic basalts may be explained

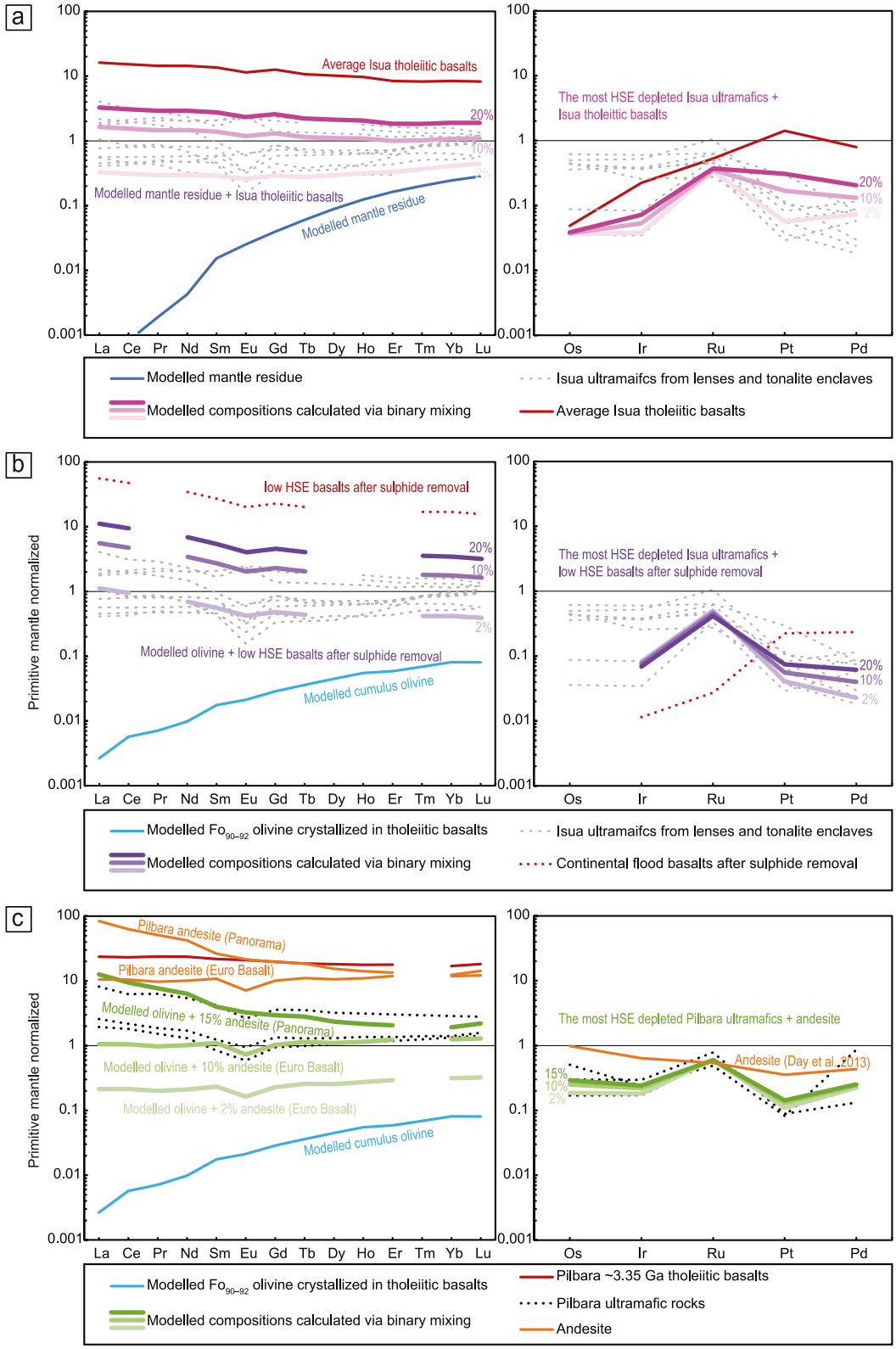

Figure 9.

by deep mantle melting and/or reduced mantle environments, which are inconsistent with a mantle wedge setting that predicts shallow mantle melting as well as relatively oxidized environments (e.g., Figure 8 of Nutman et al., 2013; Smart et al., 2016). On the other hand, retention of PGE-bearing phases in residues and generation of low HSE basalts (or komatiites) are possible via plume or heat-pipe style mantle melting (Fiorentini et al., 2011; Moore & Webb, 2013; Smithies et al., 2007; Waterton et al., 2021).

Mixing with low HSE melts formed by progressive fractional crystallization of parental basaltic magmas is another possible scenario that might explain the HSE-REE composition of Isua and Pilbara ultramafic rocks (Figure 9c). For example, in the East Pilbara Terrane, minor andesites can be found in thick (ultra)mafic to felsic volcanic successions (Smithies et al., 2007), which may be co-genetic with lava fractional crystallization. These andesites ($SiO_2 \approx 54$–61 wt.%) have flat to mildly fractionated REE patterns (Figure 9c). Binary mixing models show that 10%–15% mixing between cumulate olivine (Waterton et al., 2022). Also, a component with Pilbara andesite REE compositions can successfully reproduce REE systematics of Pilbara ultramafic rocks, especially their mildly fractionated LREE and negative Eu anomalies (Figure 9b), which cannot be accounted only by mixing with potentially coeval Pilbara tholeiitic basalts (Figure 9b). Although no HSE data are available for these andesites, limited data obtained so far for melts with similar andesitic composition (Day et al., 2013) generally indicate low HSE contents in such a melt type (e.g., Pt and Pd < 3.1 ppb). Thus, we envision that REE/HSE abundances of Pilbara ultramafic rocks can be best explained by mixing with Pilbara andesites (Figure 9b). Similarly evolved, but now altered andesitic rocks exist in the Isua supracrustal belt (Nutman et al., 2010). The enriched, fractionated REEs and negative Eu anomalies in some Isua ultramafic rocks indicate mixing with andesitic melts that are compositionally similar to Pilbara andesites (Figures 6 and 9a). Again, it remains impossible for mantle residues to become mixed with such evolved, low HSE melts generated by fractional crystallization of parental magmas during their ascent at crustal levels.

The Nb depletion relative to Th and La, which exists in both Isua ultramafic rocks and Isua basalts (Figure 7; Polat & Hofmann, 2003), has been ascribed to support melt-rock interactions with volcanic arc basalts. In this Eoarchean plate tectonic scenario, Nb and Ta depletion would indicate effects of either fluids or melting in the presence of rutile associated with progressive dehydratation and/or melting of a downgoing subducted slab (e.g., Keppler, 1996; Münker, 1998). However, this signature is not unique to volcanic arcs, particularly with respect to the early Earth. For example, basalts, felsic volcanics, TTGs, and ultramafic rocks (Figure 6c) of the East Pilbara Terrane exhibit strong Nb depletion (e.g., Martin et al., 2005; Smithies et al., 2007), whereas this terrane has been attributed to be plume-generated in a stagnant-lid tectonic setting (e.g., Van Kranendonk et al., 2007). Furthermore, rutile as well as fluids can also form during metamorphic dehydration of the lower parts of the thickened lithosphere in non-plate tectonic settings (Johnson et al., 2017), particularly in a heat-pipe lithosphere featuring cold geotherm (Moore & Webb, 2013). Recycling of such lower crust materials (which is possible in plate- and non-plate tectonic settings via mechanisms like delamination, sagduction, and/or downwards advection) and subsequent fluid flux and melting could generate igneous rocks with Nb-Ta depletion. Alternatively, Nb depletion may be a secondary signature formed via fluid metasomatism under amphibolite-facies conditions (Guice et al., 2018). Vigorous fluid activities and material exchanges between mantle and crust in non-plate tectonic settings can also explain the mantle-like $\delta^{18}O$ signatures found in some Isua olivines (Nutman, Scicchitano, et al., 2021). Mantle-like oxygen isotope values are observed in zircons from some TTGs (originally lower crust partial melts) of the East Pilbara Terrane (Smithies et al., 2021). This finding implies a fluid-rich early mantle, buffered by fluxing from the recycled crust, that was capable of introducing mantle-like oxygen isotope signatures to early crust and associated magmas (Smithies et al., 2021).

Figure 9. Primitive-mantle normalized rare earth element (REE) (McDonough & Sun, 1995) and highly siderophile element (HSE) (Becker et al., 2006) patterns of Isua (panels a, b) and Pilbara (panel b) ultramafic rocks, compared to modeled and compiled mineral and/or whole-rock compositions of potential mixing components or their chemical equivalents. Binary mixing models considered here involve one rock component (mantle residue or cumulate) and one melt component (e.g., basaltic melt). The REE compositions of mantle residue are from geochemical modeling (see Supporting Information S1). REE compositions of other rock or melt components are compiled from the literature. For HSEs, the most HSE depleted ultramafic sample in Isua or Pilbara with potentially co-genetic melts were subject to mixing to examine the corresponding changes in Pt and Pd contents. Because the HSE data for Pilbara andesites are not available, we adopt the HSE composition of andesite studied by Day et al. (2013). Mixing models show that Isua and Pilbara ultramafic rocks can be best explained by mixing between olivine-cumulates and co-genetic low HSE melts. Such low HSE melts can be formed by deep mantle melting (potentially under reduced conditions) or sulphide removal or fractional crystallization in magma chambers. REE values of modeled cumulate olivine are from Waterton et al. (2022). Average REE values of Isua tholeiitic basalts are taken from the least altered samples measured by Polat and Hofmann (2003). HSE compositions of Isua tholeiitic basalts are taken from a single sample measured by Szilas et al. (2015). Average Pilbara tholeiitic basalts and andesites are from the ~3.35 Ga Euro Basalt Formation and/or the ~3.43 Ga Panorama Formation of the East Pilbara Terrane (Smithies et al., 2007). Continental flood basalts after sulphide removal are from Lightfoot and Keays (2005) and Wooden et al. (1993).

To explain the observed REE-HSE characteristics of Isua and Pilbara ultramafic rocks, mixing with REE-enriched and HSE-depleted (relative to primitive mantle) melt is required. Possible candidates include: (a) tholeiitic basalt or komatiite derived from deep, potentially reduced mantle, likely associated with plume or heat-pipe melting; (b) crustal melts that have undergone sulphide removal; and (c) evolved melts formed through fractional crystallization of ascending parental basaltic magmas. With the exception of the first candidate, mantle residues cannot interact with these melts. The first candidate cannot interact with sub-arc depleted mantle. Alternatively, mixing cumulus olivine ± chromite ± orthopyroxene with those REE-enriched and HSE-depleted melts can explain the formation of Isua and Pilbara ultramafic rocks (Figures 6 7, and 9), along with potentially other Eoarchean ultramafic cumulates which show similar REE and HSE geochemistry (Coggon et al., 2015; McIntyre et al., 2019).

5.5. A Common Evolutionary Pathway of Early Earth Ultramafic Rocks and Its Geodynamic Implications

Isua and Pilbara ultramafic rocks could be similarly interpreted as melt and fluid-metasomatised and/or metamorphosed crustal cumulates, as their petrological and geochemical characteristics are found in other early Earth ultramafic rocks and modern cumulates (e.g., Waterton et al., 2022), but appear to be incompatible with mantle peridotites (see above). Here we describe a common evolutionary pathway for ultramafic rocks of early Earth terranes (Figure 10a). Ultramafic rocks of early Earth could have initially crystallized from high-magnesium, fluid-rich magmas, either as ultramafic volcanic flows (for example, komatiites, Byerly et al. (2019)), intrusions, or crustal cumulates at the bases of lava flows or magma chambers (Figure 10a). Some of these rocks could have experienced interactions with co-genetic, low HSE melts from the deep mantle or a magma chamber (Figure 10a). Later, these ultramafic rocks could have been metamorphosed under crustal conditions (e.g., greenschist- or amphibolite-facies conditions) that may have been associated with significant deformation and mineral phase transformation. In the case of the Isua supracrustal belt, amphibolite-facies metamorphism was accompanied by deformation, producing serpentine ± Ti-humite ± carbonate via olivine breakdown reactions (Figure 10a). Relict primary cumulate olivine could have type-B fabrics (e.g., Yao et al., 2019). In the case of East Pilbara Terrane, weaker metamorphism and deformation of Pilbara ultramafic samples led to the preserved record of low temperature metamorphism and metasomatism without identifiable strain (Figure 10a).

Such a common evolutionary pathway includes variable degrees of deformation, greenschist- to amphibolite-facies metamorphism, abundant magmatic and fluid activities, and vigorous material exchanges from surface to crust to mantle, achievable by subduction, gravitational crustal convection, and volcanic advection. Because these elements are predicted by all proposed tectonic models, including plate tectonic models (e.g., Kusky et al., 2021; Nutman, Bennett, et al., 2021) and hot stagnant-lid tectonics such as heat-pipe tectonics and partial convective overturn tectonics (see Section 2; e.g., François et al., 2014; Moore & Webb, 2013; Webb et al., 2020) (Figures 10b and 10c), preservation of phaneritic ultramafic rocks in the Isua supracrustal belt and East Pilbara Terrane cannot be used to test tectonic models and exclude operations of hot stagnant-lid tectonic regimes in the early Archean.

6. Conclusions

Some ultramafic rocks preserved in or near the Isua supracrustal belt have been interpreted as tectonically-emplaced mantle peridotites that require >3.7 Ga onset of plate tectonics (e.g., Nutman et al., 2020; Van de Löcht et al., 2018). In contrast, Pilbara ultramafic rocks and other cumulates show that crustal cumulates and mantle rocks may have similar primary rock textures and whole-rock geochemistry and igneous mineral assemblages. Differences between Isua and Pilbara ultramafic rocks may largely stem from different alterations and/or deformation experienced by these rocks, which are also consistent with crustal conditions (Waterton et al., 2022). In contrast, other characteristics of these rocks, such as certain types of spinel geochemistry (e.g., Fe–Ti trends in Cr#–Mg# space; Barnes & Roeder, 2001) and cumulate textures, appear to be unique to cumulates. Furthermore, melts that have interacted with Isua and Pilbara ultramafic rocks should be co-genetic melts generated in magma chambers or deep, potentially reduced mantle, which cannot be explained by a sub-arc mantle origin. Thus, we conclude that no features preserved in ultramafic rocks of the Isua supracrustal belt and East Pilbara Terrane are diagnostic of plate tectonic-related mantle slices, but instead, all features are compatible with crustal cumulates. This interpretation permits the previously proposed hot stagnant-lid tectonic origins for the Isua

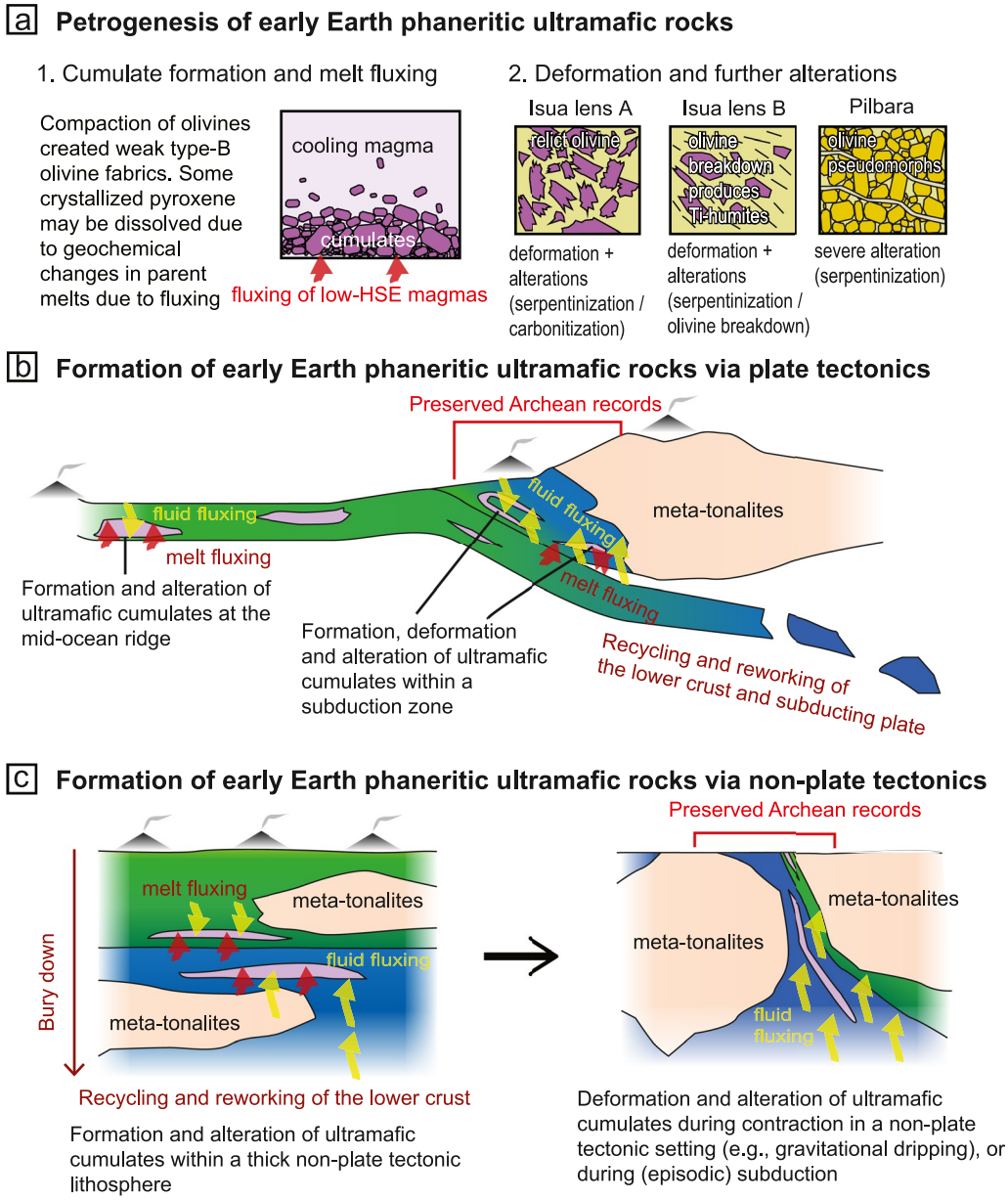

Figure 10. Evolutionary diagrams for Isua and Pilbara ultramafic rocks. Panel (a) shows a common petrogenetic pathway for these ultramafic rocks involving an origin as olivine-rich cumulates. During solidification of the cumulates, rare earth element-enriched but highly siderophile element-depleted melts interacted with cumulus phases. The cumulates were then variably deformed and altered during tectonism. Panels (b) and (c) show viable tectonic settings for the petrogenesis of the cumulates, including plate tectonic convergent (panel b) and hot stagnant-lid settings (panel c; e.g., partial convective overturn tectonics or heat-pipe tectonics) with or without later plate tectonic modification.

supracrustal belt (Figure S8 in Supporting Information S1; e.g., Ramírez-Salazar et al., 2021; Webb et al., 2020; Zuo, Webb, Piazolo, et al., 2021) and the East Pilbara Terrane (Figure S8 in Supporting Information S1; e.g., Collins et al., 1998). We note that our findings show that these rocks can neither exclude nor confirm plate tectonic origins for the formation of these two terranes (e.g., Kusky et al., 2021; Nutman et al., 2020) and do not constrain the timing of plate tectonic initiation, as regional stagnant-lid processes may have coexisted with local plate tectonic processes in early terrestrial planets (e.g., Van Kranendonk, 2010; Yin, 2012a, 2012b).

Data Availability Statement

Data sets for this research can be found in supplementary tables (Tables S1, S2, and S3) and references. Figures S1 to S8 can be found in the Supporting Information S1 file. Data sets generated by this research can also be found at the DataHub repository (https://datahub.hku.hk/) following the link https://doi.org/10.25442/hku.14220047.

Acknowledgments
We thank An Li for his sampling assistance, Martin Van Kranendonk for field logistics advice, Weiqiang Li and Weihao Yan for assistance in geochemical analyses, and Gary Byerly for insights on igneous textures and petrogenesis. Funding support comes from the American Chemical Society Petroleum Research Fund (PRF-53549-ND8), start-up funds from the University of Hong Kong, and General Research Fund of the Hong Kong Research Grants Council (17305718), all awarded to A.A.G.W. L.A. acknowledges the support of the Czech Science Foundation through the project no. 19-08066S and institutional support RVO67985831 of the Institute of Geology of the Czech Academy of Sciences. Review contributions from an anonymous reviewer and Professor Ross N. Mitchell are gratefully acknowledged.

References

Abdallah, S. E., Ali, S., & Obeid, M. A. (2019). Geochemistry of an Alaskan-type mafic-ultramafic complex in Eastern Desert, Egypt: New insights and constraints on the Neoproterozoic island arc magmatism. *Geoscience Frontiers*, *10*(3), 941–955. https://doi.org/10.1016/j.gsf.2018.04.009

Ackerman, L., Walker, R. J., Puchtel, I. S., Pitcher, L., Jelínek, E., & Strnad, L. (2009). Effects of melt percolation on highly siderophile elements and Os isotopes in subcontinental lithospheric mantle: A study of the upper mantle profile beneath central Europe. *Geochimica et Cosmochimica Acta*, *73*(8), 2400–2414. https://doi.org/10.1016/j.gca.2009.02.002

Appel, P. (1979). Stratabound copper sulfides in a banded iron-formation and in basaltic tuffs in the early Precambrian Isua supracrustal belt, West Greenland. *Economic Geology*, *74*(1), 45–52. https://doi.org/10.2113/gsecongeo.74.1.45

Arndt, N., Lesher, C., & Czamanske, G. (2005). Mantle-derived magmas and magmatic Ni-Cu-(PGE) deposits. https://doi.org/10.5382/AV100.02

Barnes, S. J., & Liu, W. (2012). Pt and Pd mobility in hydrothermal fluids: Evidence from komatiites and from thermodynamic modelling. *Ore Geology Reviews*, *44*, 49–58. https://doi.org/10.1016/j.oregeorev.2011.08.004

Barnes, S. J., & Roeder, P. L. (2001). The range of spinel compositions in terrestrial mafic and ultramafic rocks. *Journal of Petrology*, *42*(12), 2279–2302. https://doi.org/10.1093/petrology/42.12.2279

Bauer, A., Reimink, J., Chacko, T., Foley, B., Shirey, S., & Pearson, D. J. G. P. L. (2020). Hafnium isotopes in zircons document the gradual onset of mobile-lid tectonics. *Geochemical Perspectives Letters*, *14*, 1–6. https://doi.org/10.7185/geochemlet.2015

Beall, A., Moresi, L., & Cooper, C. M. (2018). Formation of cratonic lithosphere during the initiation of plate tectonics. *Geology*, *46*(6), 487–490. https://doi.org/10.1130/G39943.1

Becker, H., Horan, M., Walker, R., Gao, S., Lorand, J.-P., & Rudnick, R. (2006). Highly siderophile element composition of the Earth's primitive upper mantle: Constraints from new data on peridotite massifs and xenoliths. *Geochimica et Cosmochimica Acta*, *70*(17), 4528–4550. https://doi.org/10.1016/j.gca.2006.06.004

Bédard, J. H. (2018). Stagnant lids and mantle overturns: Implications for Archaean tectonics, magmagenesis, crustal growth, mantle evolution, and the start of plate tectonics. *Geoscience Frontiers*, *9*(1), 19–49. https://doi.org/10.1016/j.gsf.2017.01.005

Birck, J. L., Barman, M. R., & Capmas, F. (1997). Re-Os isotopic measurements at the femtomole level in natural samples. *Geostandards Newsletter*, *21*(1), 19–27. https://doi.org/10.1111/j.1751-908X.1997.tb00528.x

Bland, M. T., & McKinnon, W. B. (2016). Mountain building on Io driven by deep faulting. *Nature*, *9*(6), 429–432. https://doi.org/10.1038/ngeo2711

Bockrath, C., Ballhaus, C., & Holzheid, A. (2004). Fractionation of the platinum-group elements during mantle melting. *Science*, *305*(5692), 1951–1953. https://doi.org/10.1126/science.1100160

Borghini, G., & Rampone, E. (2007). Postcumulus processes in oceanic-type olivine-rich cumulates: The role of trapped melt crystallization versus melt/rock interaction. *Contributions to Mineralogy and Petrology*, *154*(6), 619–633. https://doi.org/10.1007/s00410-007-0217-5

Boudier, F., Ceuleneer, G., & Nicolas, A. (1988). Shear zones, thrusts and related magmatism in the Oman ophiolite: Initiation of thrusting on an oceanic ridge. *Tectonophysics*, *151*(1–4), 275–296. https://doi.org/10.1016/0040-1951(88)90249-1

Brandon, A. D., Creaser, R. A., Shirey, S. B., & Carlson, R. W. (1996). Osmium recycling in subduction zones. *Science*, *272*(5263), 861–863. https://doi.org/10.1126/science.272.5263.861

Brenan, J., Bennett, N., & Zajacz, Z. (2016). Experimental results on fractionation of the highly siderophile elements (HSE) at variable pressures and temperatures during planetary and magmatic differentiation. *Reviews in Mineralogy and Geochemistry*, *81*, 1–87. https://doi.org/10.2138/rmg.2016.81.1

Brown, M., & Johnson, T. (2018). Secular change in metamorphism and the onset of global plate tectonics. *American Mineralogist*, *103*(2), 181–196. https://doi.org/10.2138/am-2018-6166

Büchl, A., Brügmann, G., Batanova, V. G., Münker, C., & Hofmann, A. W. (2002). Melt percolation monitored by Os isotopes and HSE abundances: A case study from the mantle section of the Troodos ophiolite. *Earth and Planetary Science Letters*, *204*(3–4), 385–402. https://doi.org/10.1016/S0012-821X(02)00977-9

Byerly, G., Lowe, D., & Heubeck, C. (2019). Geologic evolution of the Barberton Greenstone Belt–a unique record of crustal development, surface processes, and early life 3.55 to 3.20 Ga. In *Earth's oldest rocks* (2nd ed.). Elsevier. https://doi.org/10.1016/B978-0-444-63901-1.00024-1

Cawood, P. A., Hawkesworth, C. J., Pisarevsky, S. A., Dhuime, B., Capitanio, F. A., & Nebel, O. (2018). Geological archive of the onset of plate tectonics. *Philosophical Transactions of the Royal Society A: Mathematical, Physical and Engineering Sciences*, *376*(2132), 20170405. https://doi.org/10.1098/rsta.2017.0405

Chadwick, B. (1990). The stratigraphy of a sheet of supracrustal rocks within high-grade orthogneisses and its bearing on Late Archaean structure in southern West Greenland. *Journal of the Geological Society*, *147*(4), 639–652. https://doi.org/10.1144/gsjgs.147.4.0639

Chen, Y., & Zhang, Y. (2009). Clinopyroxene dissolution in basaltic melt. *Geochimica et Cosmochimica Acta*, *73*(19), 5730–5747. https://doi.org/10.1016/j.gca.2009.06.016

Chin, E. J., Lee, C.-T. A., & Barnes, J. D. (2014). Thickening, refertilization, and the deep lithosphere filter in continental arcs: Constraints from major and trace elements and oxygen isotopes. *Earth and Planetary Science Letters*, *397*, 184–200. https://doi.org/10.1016/j.epsl.2014.04.022

Chin, E. J., Shimizu, K., Bybee, G. M., & Erdman, M. E. (2018). On the development of the calc-alkaline and tholeiitic magma series: A deep crustal cumulate perspective. *Earth and Planetary Science Letters*, *482*, 277–287. https://doi.org/10.1016/j.epsl.2017.11.016

Chin, E. J., Soustelle, V., & Liu, Y. (2020). An SPO-induced CPO in composite mantle xenoliths correlated with increasing melt-rock interaction. *Geochimica et Cosmochimica Acta*, *278*, 199–218. https://doi.org/10.1016/j.gca.2019.10.002

Coggon, J. A., Luguet, A., Fonseca, R. O., Lorand, J.-P., Heuser, A., & Appel, P. W. (2015). Understanding Re–Os systematics and model ages in metamorphosed Archean ultramafic rocks: A single mineral to whole-rock investigation. *Geochimica et Cosmochimica Acta*, *167*, 205–240. https://doi.org/10.1016/j.gca.2015.07.025

Cohen, A. S., & Waters, F. G. (1996). Separation of osmium from geological materials by solvent extraction for analysis by thermal ionisation mass spectrometry. *Analytica Chimica Acta*, *332*(2–3), 269–275. https://doi.org/10.1016/0003-2670(96)00226-7

Collins, W. J., Van Kranendonk, M. J., & Teyssier, C. (1998). Partial convective overturn of Archaean crust in the east Pilbara Craton, Western Australia: Driving mechanisms and tectonic implications. *Journal of Structural Geology*, *20*(9–10), 1405–1424. https://doi.org/10.1016/S0191-8141(98)00073-X

Creaser, R., Papanastassiou, D., & Wasserburg, G. (1991). Negative thermal ion mass spectrometry of osmium, rhenium and iridium. *Geochimica et Cosmochimica Acta*, *55*(1), 397–401. https://doi.org/10.1016/0016-7037(91)90427-7

Crowley, J. (2003). U–Pb geochronology of 3810–3630 Ma granitoid rocks south of the Isua greenstone belt, southern West Greenland. *Precambrian Research*, *126*(3–4), 235–257. https://doi.org/10.1016/S0301-9268(03)00097-4

Crowley, J., Myers, J., & Dunning, G. (2002). Timing and nature of multiple 3700–3600 Ma tectonic events in intrusive rocks north of the Isua greenstone belt, southern West Greenland. *The Geological Society of America Bulletin*, *114*(10), 1311–1325. https://doi.org/10.1130/0016-7606(2002)114<1311:TANOMM>2.0.CO;2

Day, J. M., Pearson, D. G., & Hulbert, L. J. (2013). Highly siderophile element behaviour during flood basalt Genesis and evidence for melts from intrusive chromitite formation in the Mackenzie large igneous province. *Lithos*, *182*, 242–258. https://doi.org/10.1016/j.lithos.2013.10.011

Deschamps, F., Godard, M., Guillot, S., & Hattori, K. (2013). Geochemistry of subduction zone serpentinites: A review. *Lithos*, *178*, 96–127. https://doi.org/10.1016/j.lithos.2013.05.019

Dymek, R. F., Boak, J. L., & Brothers, S. C. (1988). Titanian chondrodite-and titanian clinohumite-bearing metadunite from the 3800 Ma Isua supracrustal belt, West Greenland; chemistry, petrology and origin. *American Mineralogist*, *73*(5–6), 547–558. https://doi.org/10.1093/petrology/29.6.1353

Dymek, R. F., Brothers, S. C., & Schiffries, C. M. (1988). Petrogenesis of ultramafic metamorphic rocks from the 3800-Ma Isua supracrustal belt, West Greenland. *Journal of Petrology*, *29*(6), 1353–1397. https://doi.org/10.1093/petrology/29.6.1353

El Dien, H. G., Arai, S., Doucet, L.-S., Li, Z.-X., Kil, Y., Fougerouse, D., et al. (2019). Cr-spinel records metasomatism not petrogenesis of mantle rocks. *Nature Communications*, *10*(1), 1–12. https://doi.org/10.1038/s41467-019-13117-1

Elthon, D. (1992). Chemical trends in abyssal peridotites: Refertilization of depleted suboceanic mantle. *Journal of Geophysical Research*, *97*(B6), 9015–9025. https://doi.org/10.1029/92JB00723

Fiorentini, M. L., Barnes, S. J., Lesher, C. M., Heggie, G. J., Keays, R. R., & Burnham, O. M. (2010). Platinum group element geochemistry of mineralized and nonmineralized komatiites and basalts. *Economic Geology*, *105*(4), 795–823. https://doi.org/10.2113/gsecongeo.105.4.795

Fiorentini, M. L., Barnes, S. J., Maier, W. D., Burnham, O. M., & Heggie, G. (2011). Global variability in the platinum-group element contents of komatiites. *Journal of Petrology*, *52*(1), 83–112. https://doi.org/10.1093/petrology/egq074

Fischer, R., & Gerya, T. (2016). Early Earth plume-lid tectonics: A high-resolution 3D numerical modelling approach. *Journal of Geodynamics*, *100*, 198–214. https://doi.org/10.1016/j.jog.2016.03.004

Foley, B. J., Bercovici, D., & Elkins-Tanton, L. T. (2014). Initiation of plate tectonics from post-magma ocean thermochemical convection. *Journal of Geophysical Research: Solid Earth*, *119*(11), 8538–8561. https://doi.org/10.1002/2014JB011121

François, C., Philippot, P., Rey, P., & Rubatto, D. (2014). Burial and exhumation during Archean sagduction in the East Pilbara granite-greenstone terrane. *Earth and Planetary Science Letters*, *396*, 235–251. https://doi.org/10.1016/j.epsl.2014.04.025

Friend, C. R. L., Bennett, V. C., & Nutman, A. P. (2002). Abyssal peridotites > 3,800 Ma from southern West Greenland: Field relationships, petrography, geochronology, whole-rock and mineral chemistry of dunite and harzburgite inclusions in the Itsaq Gneiss complex. *Contributions to Mineralogy and Petrology*, *143*(1), 71–92. https://doi.org/10.1007/s00410-001-0332-7

Friend, C. R. L., & Nutman, A. P. (2011). Dunites from Isua, Greenland: A ca. 3720 Ma window into subcrustal metasomatism of depleted mantle. *Geology*, *39*(7), 663–666. https://doi.org/10.1130/G31904.1

Gale, A., Dalton, C. A., Langmuir, C. H., Su, Y. J., & Schilling, J. G. (2013). The mean composition of ocean ridge basalts. *Geochemistry, Geophysics, Geosystems*, *14*(3), 489–518. https://doi.org/10.1029/2012GC004334

Gannoun, A., Burton, K. W., Day, J. M., Harvey, J., Schiano, P., & Parkinson, I. (2016). Highly siderophile element and Os isotope systematics of volcanic rocks at divergent and convergent plate boundaries and in intraplate settings. *Reviews in Mineralogy and Geochemistry*, *81*(1), 651–724. https://doi.org/10.2138/rmg.2016.81.11

Garuti, G., Pushkarev, E. V., Zaccarini, F., Cabella, R., & Anikina, E. (2003). Chromite composition and platinum-group mineral assemblage in the Uktus Uralian-Alaskan-type complex (Central Urals, Russia). *Mineralium Deposita*, *38*(3), 312–326. https://doi.org/10.1007/s00126-003-0348-1

Geological Survey of Western Australia 2013 Database. (2013). 1:100000 GIS Pilbara 2013 update/Geological Survey of Western Australia. In *Geological Survey of Western Australia, East Perth, Western Australia ©2013*. Exploration Incentive Scheme, Department of Mines and Petroleum.

Goodrich, C. A., Fioretti, A. M., Tribaudino, M., & Molin, G. (2001). Primary trapped melt inclusions in olivine in the olivine-augite-orthopyroxene ureilite Hughes 009. *Geochimica et Cosmochimica Acta*, *65*(4), 621–652. https://doi.org/10.1016/S0016-7037(00)00521-4

Gordeychik, B., Churikova, T., Kronz, A., Sundermeyer, C., Simakin, A., & Wörner, G. (2018). Growth of, and diffusion in, olivine in ultra-fast ascending basalt magmas from Shiveluch volcano. *Scientific Reports*, *8*(1), 1–15. https://doi.org/10.1038/s41598-018-30133-1

Guice, G., McDonald, I., Hughes, H., Schlatter, D., Goodenough, K., MacDonald, J., & Faithfull, J. (2018). Assessing the validity of negative high field strength-element anomalies as a proxy for Archaean subduction: Evidence from the Ben Strome Complex, NW Scotland. *Geosciences*, *8*(9), 338. https://doi.org/10.3390/geosciences8090338

Guotana, J. M., Morishita, T., Nishio, I., Tamura, A., Mizukami, T., Tani, K., et al. (2022). Deserpentinization and high-pressure (eclogite-facies) metamorphic features in the Eoarchean ultramafic body from Isua, Greenland. *Geoscience Frontiers*, *13*(1), 101298. https://doi.org/10.1016/j.gsf.2021.101298

Hanghøj, K., Kelemen, P. B., Hassler, D., & Godard, M. (2010). Composition and Genesis of depleted mantle peridotites from the Wadi Tayin massif, Oman ophiolite; major and trace element geochemistry, and Os isotope and PGE systematics. *Journal of Petrology*, *51*(1–2), 201–227. https://doi.org/10.1093/petrology/egp077

Harrison, T. M. (2009). The Hadean crust: Evidence from >4 Ga zircons. *Annual Review of Earth and Planetary Sciences*, *37*(1), 479–505. https://doi.org/10.1146/annurev.earth.031208.100151

Hickman, A. H. (2021). East Pilbara Craton: A record of one billion years in the growth of Archean continental crust. In *Geological Survey of Western Australia, Report* (Vol. *143*, pp. 1–187).

Himmelberg, G. R., & Loney, R. A. (1995). *Characteristics and petrogenesis of Alaskan-type ultramafic-mafic intrusions, southeastern Alaska*. US Government Printing Office. https://doi.org/10.3133/pp1564

Holtzman, B. K., Kohlstedt, D. L., Zimmerman, M. E., Heidelbach, F., Hiraga, T., & Hustoft, J. (2003). Melt segregation and strain partitioning: Implications for seismic anisotropy and mantle flow. *Science*, *301*(5637), 1227–1230. https://doi.org/10.1126/science.1087132

Hopkins, M., Harrison, T. M., & Manning, C. E. (2008). Low heat flow inferred from >4 Gyr zircons suggests Hadean plate boundary interactions. *Nature*, *456*(7221), 493–496. https://doi.org/10.1038/nature07465

Hunter, R. (1996). Texture development in cumulate rocks. In *Developments in petrology* (pp. 77–101). Elsevier. https://doi.org/10.1016/S0167-2894(96)80005-4

Ionov, D. A. (2010). Petrology of mantle wedge lithosphere: New data on supra-subduction zone peridotite xenoliths from the andesitic Avacha volcano, Kamchatka. *Journal of Petrology*, *51*(1–2), 327–361. https://doi.org/10.1093/petrology/egp090

Ishikawa, A., Suzuki, K., Collerson, K. D., Liu, J., Pearson, D. G., & Komiya, T. (2017). Rhenium-osmium isotopes and highly siderophile elements in ultramafic rocks from the Eoarchean Saglek Block, northern Labrador, Canada: Implications for Archean mantle evolution. *Geochimica et Cosmochimica Acta*, *216*, 286–311. https://doi.org/10.1016/j.gca.2017.07.023

Janoušek, V., Farrow, C. M., & Erban, V. (2006). Interpretation of whole-rock geochemical data in igneous geochemistry: Introducing Geochemical Data Toolkit (GCDkit). *Journal of Petrology*, *47*(6), 1255–1259. https://doi.org/10.1093/petrology/egl013

Johannsen, A. (1931). *A descriptive petrography of the igneous rocks: Introduction, textures, classifications and glossary*. University of Chicago Press.

Johnson, D., Hooper, P., & Conrey, R. (1999). XRF method XRF analysis of rocks and minerals for major and trace elements on a single low dilution Li-Tetraborate fused Bead. *Advances in X-Ray Analysis*, *41*, 843–867.

Johnson, T. E., Brown, M., Gardiner, N. J., Kirkland, C. L., & Smithies, R. H. (2017). Earth's first stable continents did not form by subduction. *Nature*, *543*(7644), 239–242. https://doi.org/10.1038/nature21383

Johnson, T. E., Brown, M., Kaus, B. J. P., & VanTongeren, J. A. (2014). Delamination and recycling of Archaean crust caused by gravitational instabilities. *Nature Geoscience*, *7*(1), 47–52. https://doi.org/10.1038/Ngeo2019

Kaczmarek, M. A., Reddy, S. M., Nutman, A. P., Friend, C. R. L., & Bennett, V. C. (2016). Earth's oldest mantle fabrics indicate Eoarchaean subduction. *Nature Communications*, *7*(1), 10665. https://doi.org/10.1038/ncomms10665

Kelemen, P. B. (1990). Reaction between ultramafic rock and fractionating basaltic magma I. Phase relations, the origin of calc-alkaline magma series, and the formation of discordant dunite. *Journal of Petrology*, *31*(1), 51–98. https://doi.org/10.1093/petrology/31.1.51

Kelemen, P. B., Dick, H. J., & Quick, J. E. (1992). Formation of harzburgite by pervasive melt/rock reaction in the upper mantle. *Nature*, *358*(6388), 635–641. https://doi.org/10.1038/358635a0

Keppler, H. (1996). Constraints from partitioning experiments on the composition of subduction-zone fluids. *Nature*, *380*(6571), 237–240. https://doi.org/10.1038/380237a0

Khedr, M. Z., Arai, S., Python, M., & Tamura, A. (2014). Chemical variations of abyssal peridotites in the central Oman ophiolite: Evidence of oceanic mantle heterogeneity. *Gondwana Research*, *25*(3), 1242–1262. https://doi.org/10.1016/j.gr.2013.05.010

Kirkland, C., Hartnady, M., Barham, M., Olierook, H., Steenfelt, A., & Hollis, J. (2021). Widespread reworking of Hadean-to-Eoarchean continents during Earth's thermal peak. *Nature Communications*, *12*(1), 1–9. https://doi.org/10.1038/s41467-020-20514-4

Knaack, C., Cornelius, S., & Hooper, P. (1994). *Trace element analyses of rocks and minerals by ICP-MS* (Vol. 2, p. 18). Geoanalytical Laboratory, Washington State University.

Korenaga, J. (2011). Thermal evolution with a hydrating mantle and the initiation of plate tectonics in the early Earth. *Journal of Geophysical Research*, *116*(B12), B12403. https://doi.org/10.1029/2011JB008410

Krause, J., Brügmann, G., & Pushkarev, E. (2011). Chemical composition of spinel from Uralian-Alaskan-type Mafic–Ultramafic complexes and its petrogenetic significance. *Contributions to Mineralogy and Petrology*, *161*(2), 255–273. https://doi.org/10.1007/s00410-010-0530-2

Kusky, T., Windley, B. F., Polat, A., Wang, L., Ning, W., & Zhong, Y. (2021). Archean dome-and-basin style structures form during growth and death of intraoceanic and continental margin arcs in accretionary orogens. *Earth-Science Reviews*, *220*, 103725. https://doi.org/10.1016/j.earscirev.2021.103725

Lenardic, A. (2018). The diversity of tectonic modes and thoughts about transitions between them. *Philosophical Transactions of the Royal Society A: Mathematical, Physical & Engineering Sciences*, *376*(2132), 20170416. https://doi.org/10.1098/rsta.2017.0416

Lightfoot, P. C., & Keays, R. R. (2005). Siderophile and chalcophile metal variations in flood basalts from the Siberian trap, Noril'sk region: Implications for the origin of the Ni-Cu-PGE sulfide ores. *Economic Geology*, *100*(3), 439–462. https://doi.org/10.2113/gsecongeo.100.3.439

Lundeen, M. T. (1978). Emplacement of the Ronda peridotite, Sierra Bermeja, Spain. *The Geological Society of America Bulletin*, *89*(2), 172–180. https://doi.org/10.1130/0016-7606(1978)89<172:EOTRPS>2.0.CO;2

Mallik, A., Lambart, S., & Chin, E. J. (2020). Tracking the evolution of magmas from heterogeneous mantle sources to eruption. In *Mantle convection and surface expressions, AGU monograph series*. Retrieved from https://arxiv.org/abs/2001.00928

Malvoisin, B. (2015). Mass transfer in the oceanic lithosphere: Serpentinization is not isochemical. *Earth and Planetary Science Letters*, *430*, 75–85. https://doi.org/10.1016/j.epsl.2015.07.043

Marchi, S., Bottke, W., Elkins-Tanton, L., Bierhaus, M., Wuennemann, K., Morbidelli, A., & Kring, D. (2014). Widespread mixing and burial of Earth's Hadean crust by asteroid impacts. *Nature*, *511*(7511), 578–582. https://doi.org/10.1038/nature13539

Martin, H., Smithies, R., Rapp, R., Moyen, J.-F., & Champion, D. (2005). An overview of adakite, tonalite-trondhjemite-granodiorite (TTG), and sanukitoid: Relationships and some implications for crustal evolution. *Lithos*, *79*(1–2), 1–24. https://doi.org/10.1016/j.lithos.2004.04.048

McDonough, W. F., & Sun, S. S. (1995). The composition of the Earth. *Chemical Geology*, *120*(3–4), 223–253. https://doi.org/10.1016/0009-2541(94)00140-4

McIntyre, T., Pearson, D., Szilas, K., & Morishita, T. (2019). Implications for the origins of Eoarchean ultramafic rocks of the North Atlantic Craton: A study of the Tussaap Ultramafic complex, Itsaq Gneiss complex, southern West Greenland. *Contributions to Mineralogy and Petrology*, *174*(12), 1–21. https://doi.org/10.1007/s00410-019-1628-9

Miocevich, S. R., Copley, A., & Weller, O. M. (2022). Testing the importance of sagduction: Insights from the Lewisian Gneiss complex of northwest Scotland. *Precambrian Research*, *379*, 106708. https://doi.org/10.1016/j.precamres.2022.106708

Moore, W. B., Simon, J. I., & Webb, A. A. G. (2017). Heat-pipe planets. *Earth and Planetary Science Letters*, *474*, 13–19. https://doi.org/10.1016/j.epsl.2017.06.015

Moore, W. B., & Webb, A. A. G. (2013). Heat-pipe earth. *Nature*, *501*(7468), 501–505. https://doi.org/10.1038/nature12473

Münker, C. (1998). Nb/Ta fractionation in a Cambrian arc/back arc system, New Zealand: Source constraints and application of refined ICPMS techniques. *Chemical Geology*, *144*(1–2), 23–45. https://doi.org/10.1016/S0009-2541(97)00105-8

Næraa, T., Schersten, A., Rosing, M. T., Kemp, A. I. S., Hoffmann, J. E., Kokfelt, T. F., & Whitehouse, M. J. (2012). Hafnium isotope evidence for a transition in the dynamics of continental growth 3.2 Gyr ago. *Nature*, *485*(7400), 627–630. https://doi.org/10.1038/nature11140

Nagaya, T., Wallis, S. R., Kobayashi, H., Michibayashi, K., Mizukami, T., Seto, Y., et al. (2014). Dehydration breakdown of antigorite and the formation of B-type olivine CPO. *Earth and Planetary Science Letters*, *387*, 67–76. https://doi.org/10.1016/j.epsl.2013.11.025

Niu, Y. L., & Hekinian, R. (1997). Basaltic liquids and harzburgitic residues in the Garrett Transform: A case study at fast-spreading ridges. *Earth and Planetary Science Letters*, *146*(1–2), 243–258. https://doi.org/10.1016/S0012-821X(96)00218-X

Niu, Y. L., & Hekinian, R. (2004). Bulk-rock major and trace element compositions of abyssal peridotites: Implications for mantle melting, melt extraction and post-melting processes beneath mid-ocean ridges. *Journal of Petrology*, *45*(12), 2423–2458. https://doi.org/10.1016/S0012-821X(96)00218-X

Nutman, A. P. (1986). The early Archaean to Proterozoic history of the Isukasia area, southern West Greenland. *Bulletin Gronlands Geologiske Undersogelse*, *154*, 1–80. https://doi.org/10.34194/bullggu.v154.6696

Nutman, A. P., Bennett, V. C., & Friend, C. R. (2013). *The emergence of the Eoarchaean proto-arc: Evolution of a c. 3700 Ma convergent plate boundary at Isua, southern West Greenland* (Vol. 389, p. 385). Geological Society, London, Special Publications. https://doi.org/10.1144/SP389.5

Nutman, A. P., Bennett, V. C., Friend, C. R., & Yi, K. (2020). *Eoarchean contrasting ultra-high-pressure to low-pressure metamorphisms (<250 to >1000°C/GPa) explained by tectonic plate convergence in deep time* (p. 105770). Precambrian Research. https://doi.org/10.1016/j.precamres.2020.105770

Nutman, A. P., Bennett, V. C., Friend, C. R., Yi, K., & Lee, S. R. (2015). Mesoarchaean collision of Kapisilik terrane 3070 Ma juvenile arc rocks and >3600 Ma Isukasia terrane continental crust (Greenland). *Precambrian Research*, *258*, 146–160. https://doi.org/10.1016/j.precamres.2014.12.013

Nutman, A. P., Bennett, V. C., Friend, C. R. L., Polat, A., Hoffmann, E., & Van Kranendonk, M. (2021). Fifty years of the Eoarchean and the case for evolving uniformitarianism. *Precambrian Research*, *367*, 106442. https://doi.org/10.1016/j.precamres.2021.106442

Nutman, A. P., Friend, C. R., Bennett, V. C., Wright, D., & Norman, M. D. (2010). ≥ 3700 Ma pre-metamorphic dolomite formed by microbial mediation in the Isua supracrustal belt (W. Greenland): Simple evidence for early life? *Precambrian Research*, *183*(4), 725–737. https://doi.org/10.1016/j.precamres.2010.08.006

Nutman, A. P., & Friend, C. R. L. (2009). New 1:20,000 scale geological maps, synthesis and history of investigation of the Isua supracrustal belt and adjacent orthogneisses, southern West Greenland: A glimpse of Eoarchaean crust formation and orogeny. *Precambrian Research*, *172*(3–4), 189–211. https://doi.org/10.1016/j.precamres.2009.03.017

Nutman, A. P., Friend, C. R. L., & Bennett, V. C. (2002). Evidence for 3650-3600 Ma assembly of the northern end of the Itsaq Gneiss complex, Greenland: Implication for early Archaean tectonics. *Tectonics*, *21*(1), 5-1–5-28. https://doi.org/10.1029/2000TC001203

Nutman, A. P., McGregor, V. R., Friend, C. R. L., Bennett, V. C., & Kinny, P. D. (1996). The Itsaq gneiss complex of southern West Greenland; the world's most extensive record of early crustal evolution (3900–3600 Ma). *Precambrian Research*, *78*(1–3), 1–39. https://doi.org/10.1016/0301-9268(95)00066-6

Nutman, A. P., Scicchitano, M. R., Friend, C. R., Bennett, V. C., & Chivas, A. R. (2021). Isua (Greenland) ∼3700 Ma meta-serpentinite olivine Mg# and $\delta^{18}O$ signatures show connection between the early mantle and hydrosphere: Geodynamic implications. *Precambrian Research*, *361*, 106249. https://doi.org/10.1016/j.precamres.2021.106249

O'Neill, C., & Debaille, V. (2014). The evolution of Hadean–Eoarchaean geodynamics. *Earth and Planetary Science Letters*, *406*, 49–58. https://doi.org/10.1016/j.epsl.2014.08.034

O'Neill, H. S. C., & Mavrogenes, J. A. (2002). The sulfide capacity and the sulfur content at sulfide saturation of silicate melts at 1400°C and 1 bar. *Journal of Petrology*, *43*(6), 1049–1087. https://doi.org/10.1093/petrology/43.6.1049

O'Reilly, T. C., & Davies, G. F. (1981). Magma transport of heat on Io: A mechanism allowing a thick lithosphere. *Geophysical Research Letters*, *8*(4), 313–316. https://doi.org/10.1029/GL008i004p00313

Parkinson, I. J., & Pearce, J. A. (1998). Peridotites from the Izu–Bonin–Mariana forearc (ODP Leg 125): Evidence for mantle melting and melt–mantle interaction in a supra-subduction zone setting. *Journal of Petrology*, *39*(9), 1577–1618. https://doi.org/10.1093/petroj/39.9.1577

Paulick, H., Bach, W., Godard, M., De Hoog, J. C. M., Suhr, G., & Harvey, J. (2006). Geochemistry of abyssal peridotites (Mid-Atlantic Ridge, 15 degrees 20'N, ODP Leg 209): Implications for fluid/rock interaction in slow spreading environments. *Chemical Geology*, *234*(3–4), 179–210. https://doi.org/10.1016/j.chemgeo.2006.04.011

Pearce, J. A., & Reagan, M. K. (2019). Identification, classification, and interpretation of boninites from Anthropocene to Eoarchean using Si-Mg-Ti systematics. *Geosphere*, *15*(4), 1008–1037. https://doi.org/10.1130/GES01661.1

Polat, A., & Hofmann, A. W. (2003). Alteration and geochemical patterns in the 3.7–3.8 Ga Isua greenstone belt, West Greenland. *Precambrian Research*, *126*(3–4), 197–218. https://doi.org/10.1016/S0301-9268(03)00095-0

Ramírez-Salazar, A., Müller, T., Piazolo, S., Webb, A. A. G., Hauzenberger, C., Zuo, J., et al. (2021). Tectonics of the Isua supracrustal belt 1: P-T-X-d constraints of a poly-metamorphic terrane. *Tectonics*, *40*(3), e2020TC006516. https://doi.org/10.1029/2020tc006516

Ramírez-Salazar, A., Zuo, J., Müller, T., Webb, A. A. G., Sorger, D., Piazolo, S., et al. (2022). Reply to Comment by A.P. Nutman et al. on "Tectonics of the Isua Supracrustal Belt 1: P-T-X-d Constraints of a Poly-Metamorphic Terrane" by A. Ramírez-Salazar et al. and "Tectonics of the Isua Supracrustal Belt 2: Microstructures Reveal Distributed Strain in the Absence of Major Fault Structures" by J. Zuo et al. *Tectonics*, *41*(5), e2021TC007148. https://doi.org/10.1029/2021TC007148

Reimink, J. R., Davies, J. H., Bauer, A. M., & Chacko, T. (2020). A comparison between zircons from the Acasta Gneiss complex and the Jack Hills region. *Earth and Planetary Science Letters*, *531*, 115975. https://doi.org/10.1016/j.epsl.2019.115975

Shen, T., Hermann, J., Zhang, L., Lü, Z., Padrón-Navarta, J. A., Xia, B., & Bader, T. (2015). UHP metamorphism documented in Ti-chondrodite-and Ti-clinohumite-bearing serpentinized ultramafic rocks from Chinese southwestern Tianshan. *Journal of Petrology*, *56*(7), 1425–1458. https://doi.org/10.1093/petrology/egv042

Shirey, S. B., & Walker, R. J. (1995). Carius tube digestion for low-blank rhenium-osmium analysis. *Analytical Chemistry*, *67*(13), 2136–2141. https://doi.org/10.1021/ac00109a036

Shirey, S. B., & Walker, R. J. (1998). The Re-Os isotope system in cosmochemistry and high-temperature geochemistry. *Annual Review of Earth and Planetary Sciences*, *26*(1), 423–500. https://doi.org/10.1146/annurev.earth.26.1.423

Smart, K. A., Tappe, S., Stern, R. A., Webb, S. J., & Ashwal, L. D. (2016). Early Archaean tectonics and mantle redox recorded in Witwatersrand diamonds. *Nature Geoscience*, *9*(3), 255–259. https://doi.org/10.1038/ngeo2628

Smithies, R., Champion, D., Van Kranendonk, M., & Hickman, A. (2007). Geochemistry of volcanic rocks of the northern Pilbara Craton, Western Australia. In *Geological Survey of Western Australia Report* (Vol. *104*).

Smithies, R. H., Lu, Y., Kirkland, C. L., Johnson, T. E., Mole, D. R., Champion, D. C., et al. (2021). Oxygen isotopes trace the origins of Earth's earliest continental crust. *Nature*, *592*(7852), 70–75. https://doi.org/10.1038/s41586-021-03337-1

Standish, J., Hart, S., Blusztajn, J., Dick, H., & Lee, K. (2002). Abyssal peridotite osmium isotopic compositions from cr-spinel. *Geochemistry, Geophysics, Geosystems*, *3*(1), 1–24. https://doi.org/10.1029/2001GC000161

Stern, R. J. (2008). Modern-style plate tectonics began in Neoproterozoic time: An alternative interpretation of Earth's tectonic history. *When did plate tectonics begin on planet Earth*, *265*, 280. https://doi.org/10.1130/2008.2440(13)

Stern, R. J., Gerya, T., & Tackley, P. J. (2017). Stagnant lid tectonics: Perspectives from silicate planets, dwarf planets, large moons, and large asteroids. *Geoscience Frontiers*, *9*(1), 103–119. https://doi.org/10.1016/j.gsf.2017.06.004

Szilas, K., Kelemen, P. B., & Rosing, M. T. (2015). The petrogenesis of ultramafic rocks in the >3.7 Ga Isua supracrustal belt, southern West Greenland: Geochemical evidence for two distinct magmatic cumulate trends. *Gondwana Research*, *28*(2), 565–580. https://doi.org/10.1016/j.gr.2014.07.010

Szilas, K., Van Hinsberg, V., McDonald, I., Næraa, T., Rollinson, H., Adetunji, J., & Bird, D. (2018). Highly refractory Archaean peridotite cumulates: Petrology and geochemistry of the Seqi Ultramafic Complex, SW Greenland. *Geoscience Frontiers*, *9*(3), 689–714. https://doi.org/10.1016/j.gsf.2017.05.003

Szilas, K., Van Hinsberg, V. J., Creaser, R. A., & Kisters, A. F. M. (2014). The geochemical composition of serpentinites in the Mesoarchaean Tartoq Group, SW Greenland: Harzburgitic cumulates or melt-modified mantle? *Lithos*, *198*, 103–116. https://doi.org/10.1016/j.lithos.2014.03.024

Tamura, A., & Arai, S. (2006). Harzburgite-dunite-orthopyroxenite suite as a record of supra-subduction zone setting for the Oman ophiolite mantle. *Lithos*, *90*(1–2), 43–56. https://doi.org/10.1016/j.lithos.2005.12.012

Tang, C., Webb, A., Moore, W., Wang, Y., Ma, T., & Chen, T. (2020). Breaking Earth's shell into a global plate network. *Nature Communications*, *11*(1), 1–6. https://doi.org/10.1038/s41467-020-17480-2

Thakurta, J., Ripley, E. M., & Li, C. (2008). Geochemical constraints on the origin of sulfide mineralization in the Duke Island Complex, southeastern Alaska. *Geochemistry, Geophysics, Geosystems*, *9*(7), Q07003. https://doi.org/10.1029/2008GC001982

Topuz, G., Hegner, E., Homam, S. M., Ackerman, L., Pfänder, J. A., & Karimi, H. (2018). Geochemical and geochronological evidence for a Middle Permian oceanic plateau fragment in the Paleo-Tethyan suture zone of NE Iran. *Contributions to Mineralogy and Petrology*, *173*(10), 81. https://doi.org/10.1007/s00410-018-1506-x

Van de Löcht, J., Hoffmann, J., Li, C., Wang, Z., Becker, H., Rosing, M. T., et al. (2018). Earth's oldest mantle peridotites show entire record of late accretion. *Geology*, *46*(3), 199–202. https://doi.org/10.1130/G39709.1

Van de Löcht, J., Hoffmann, J., Rosing, M., Sprung, P., & Münker, C. (2020). Preservation of Eoarchean mantle processes in ~3.8 Ga peridotite enclaves in the Itsaq Gneiss complex, southern West Greenland. *Geochimica et Cosmochimica Acta*, *280*, 1–25. https://doi.org/10.1016/j.gca.2020.03.043

Van Kranendonk, M. J. (2010). Two types of Archean continental crust: Plume and plate tectonics on early Earth. *American Journal of Science*, *310*(10), 1187–1209. https://doi.org/10.2475/10.2010.01

Van Kranendonk, M. J., Collins, W. J., Hickman, A., & Pawley, M. J. (2004). Critical tests of vertical vs. horizontal tectonic models for the Archaean East Pilbara granite-greenstone terrane, Pilbara Craton, Western Australia. *Precambrian Research*, *131*(3–4), 173–211. https://doi.org/10.1016/j.precamres.2003.12.015

Van Kranendonk, M. J., Smithies, R. H., Hickman, A. H., & Champion, D. C. (2007). Review: Secular tectonic evolution of Archean continental crust: Interplay between horizontal and vertical processes in the formation of the Pilbara Craton, Australia. *Terra Nova*, *19*(1), 1–38. https://doi.org/10.1111/j.1365-3121.2006.00723.x

Völkening, J., Walczyk, T., & Heumann, K. G. (1991). Osmium isotope ratio determinations by negative thermal ionization mass spectrometry. *International Journal of Mass Spectrometry and Ion Processes*, *105*(2), 147–159. https://doi.org/10.1016/0168-1176(91)80077-Z

Wager, L. R., & Brown, G. M. (1967). *Layered igneous rocks*. WH Freeman.

Wal, D. V. d., & Vissers, R. L. (1993). Uplift and emplacement of upper mantle rocks in the western Mediterranean. *Geology*, *21*(12), 1119–1122. https://doi.org/10.1130/0091-7613(1993)021<1119:UAEOUM>2.3.CO;2

Wang, Z., Becker, H., & Gawronski, T. (2013). Partial re-equilibration of highly siderophile elements and the chalcogens in the mantle: A case study on the Baldissero and Balmuccia peridotite massifs (Ivrea Zone, Italian Alps). *Geochimica et Cosmochimica Acta*, *108*, 21–44. https://doi.org/10.1016/j.gca.2013.01.021

Waterton, P., Guotana, J. M., Nishio, I., Morishita, T., Tani, K., Woodland, S., et al. (2022). No mantle residues in the Isua supracrustal belt. *Earth and Planetary Science Letters*, *579*, 117348. https://doi.org/10.1016/j.epsl.2021.117348

Waterton, P., Mungall, J., & Pearson, D. G. (2021). The komatiite-mantle platinum-group element paradox. *Geochimica et Cosmochimica Acta*, *313*, 214–242. https://doi.org/10.1016/j.gca.2021.07.037

Webb, A. A. G., Müller, T., Zuo, J., Haproff, P. J., & Ramírez-Salazar, A. (2020). A non-plate tectonic model for the Eoarchean Isua supracrustal belt. *Lithosphere*, *12*(1), 166–179. https://doi.org/10.1130/L1130.1

Wiemer, D., Schrank, C., Murphy, D., Wenham, L., & Allen, C. (2018). Earth's oldest stable crust in the Pilbara Craton formed by cyclic gravitational overturns. *Nature Geoscience*, *11*(5), 357–361. https://doi.org/10.1038/s41561-018-0105-9

Williams, I. R. (1999). *Geology of the Muccan 1:100000 sheet*. Geological Survey of Western Australia.

Wooden, J. L., Czamanske, G. K., Fedorenko, V. A., Arndt, N. T., Chauvel, C., Bouse, R. M., et al. (1993). Isotopic and trace-element constraints on mantle and crustal contributions to Siberian continental flood basalts, Noril'sk area, Siberia. *Geochimica et Cosmochimica Acta*, *57*(15), 3677–3704. https://doi.org/10.1016/0016-7037(93)90149-Q

Yao, Z., Qin, K., Wang, Q., & Xue, S. (2019). Weak B-type olivine fabric induced by fast compaction of crystal Mush in a crustal magma Reservoir. *Journal of Geophysical Research: Solid Earth*, *124*(4), 3530–3556. https://doi.org/10.1029/2018JB016728

Yin, A. (2012a). An episodic slab-rollback model for the origin of the Tharsis rise on Mars: Implications for initiation of local plate subduction and final unification of a kinematically linked global plate-tectonic network on Earth. *Lithosphere*, *4*(6), 553–593. https://doi.org/10.1130/L195.1

Yin, A. (2012b). Structural analysis of the Valles Marineris fault zone: Possible evidence for large-scale strike-slip faulting on Mars. *Lithosphere*, *4*(4), 286–330. https://doi.org/10.1130/L192.1

Zuo, J., Webb, A. A. G., Johnson, T. E., McKenzie, N. R., Kirkland, C. L., Ng, H. C., & Lo, C. Y. (2021). Model versus measured detrital zircon age signatures of the early Earth. *Earth and Planetary Science Letters*, *575*, 117182. https://doi.org/10.1016/j.epsl.2021.117182

Zuo, J., Webb, A. A. G., Piazolo, S., Wang, Q., Müller, T., Ramírez-Salazar, A., & Haproff, P. J. (2021). Tectonics of the Isua supracrustal belt 2: Microstructures reveal distributed strain in the absence of major fault structures. *Tectonics*, *40*(3), e2020TC006514. https://doi.org/10.1029/2020tc006514

References From the Supporting Information

Aldanmaz, E., & Koprubasi, N. (2006). Platinum-group-element systematics of peridotites from ophiolite complexes of northwest anatolia, Turkey: Implications for mantle metasomatism by melt percolation in a supra-subduction zone environment. *International Geology Review*, *48*(5), 420–442. https://doi.org/10.2747/0020-6814.48.5.420

Barnes, S. J., Mole, D. R., Le Vaillant, M., Campbell, M. J., Verrall, M. R., Roberts, M. P., & Evans, N. J. (2016). Poikilitic textures, heteradcumulates and zoned orthopyroxenes in the Ntaka ultramafic complex, Tanzania: Implications for crystallization mechanisms of oikocrysts. *Journal of Petrology*, *57*(6), 1171–1198. https://doi.org/10.1093/petrology/egw036

Chen, B.-Y., Yu, J.-J., & Liu, S.-J. (2018). Source characteristics and tectonic setting of mafic–ultramafic intrusions in North Xinjiang, NW China: Insights from the petrology and geochemistry of the Lubei mafic–ultramafic intrusion. *Lithos*, *308*, 329–345. https://doi.org/10.1016/j.lithos.2018.03.016

Herzberg, C., Condie, K., & Korenaga, J. (2010). Thermal history of the Earth and its petrological expression. *Earth and Planetary Science Letters*, *292*(1–2), 79–88. https://doi.org/10.1016/j.epsl.2010.01.022

Jagoutz, E., Palme, H., Baddenhausen, H., Blum, K., Cendales, M., Dreibus, G., et al. (1979). The abundances of major, minor and trace elements in the Earth's mantle as derived from primitive ultramafic nodules. In *Lunar and Planetary Science Conference Proceedings* (pp. 2031–2050).

Khatun, S., Mondal, S. K., Zhou, M.-F., Balaram, V., & Prichard, H. M. (2014). Platinum-group element (PGE) geochemistry of Mesoarchean ultramafic–mafic cumulate rocks and chromitites from the Nuasahi Massif, Singhbhum Craton (India). *Lithos*, *205*, 322–340. https://doi.org/10.1016/j.lithos.2014.07.013

Lee, C.-T. A., Harbert, A., & Leeman, W. P. (2007). Extension of lattice strain theory to mineral/mineral rare-Earth element partitioning: An approach for assessing disequilibrium and developing internally consistent partition coefficients between olivine, orthopyroxene, clinopyroxene and basaltic melt. *Geochimica et Cosmochimica Acta*, *71*(2), 481–496. https://doi.org/10.1016/j.gca.2006.09.014

Maier, W. D., Roelofse, F., & Barnes, S.-J. (2003). The concentration of the platinum-group elements in South African komatiites: Implications for mantle sources, melting regime and PGE fractionation during crystallization. *Journal of Petrology*, *44*(10), 1787–1804. https://doi.org/10.1093/petrology/egg059

Marchesi, C., Garrido, C. J., Proenza, J. A., Hidas, K., Varas-Reus, M. I., Butjosa, L., & Lewis, J. F. (2016). Geochemical record of subduction initiation in the sub-arc mantle: Insights from the Loma Caribe peridotite (Dominican Republic). *Lithos*, *252*, 1–15. https://doi.org/10.1016/j.lithos.2016.02.009

McDade, P., Blundy, J. D., & Wood, B. J. (2003). Trace element partitioning between mantle wedge peridotite and hydrous MgO-rich melt. *American Mineralogist*, *88*(11–12), 1825–1831. https://doi.org/10.2138/am-2003-11-1225

Schwandt, C. S., & McKay, G. A. (1998). Rare Earth element partition coefficients from enstatite/melt synthesis experiments. *Geochimica et Cosmochimica Acta*, *62*(16), 2845–2848. https://doi.org/10.1016/S0016-7037(98)00233-6